CHAPTER 4

RESULTS AND DISCUSSION

4. Results and discussion

Section -A

4.1 Adsorption of Cr (VI) by mango seed kernel activated carbon (MKAC)

4.1.1 Characterization of activated carbon

The pHpzc value of the MKAC was found to be 6.8, which indicates that at this pH the net surface charge of the adsorbent is zero, whereas at pH < 6.8, the adsorbent surface is positively charged and at pH > 6.8, it is negatively charged. The elemental analysis of mango seed kerneal and activated carbon prepared from it were carried using a CHNS analyzer. The results are listed in table 4.1.No sulfur was detected.

Table 4.1 Elemental analysis of raw mango kernel and activated mango kernel

Elemental analysis (%)	Raw mango kernel	Activated mango kernel
C	44.71	78.56
H	6.42	2.05
N	5.05	1.23
S	0	0
O	44.53	18.16

The relevant physical properties of mango seed kerneal activated carbon were experimentally determined as discussed in chapter 3 and are listed in table 4.2.High BET surface area of the adsorbent (490.43 m^2 g^{-1}) indicates MKAC to be a very good adsorbent for efficient adsorption of Cr (VI) and other pollutants from wastewater. From Table 4.1 it is seen that as expected the percent carbon content in activated carbon

(78%) is substantially higher than that of green mango seed kernel. This is nearly comparable to the carbon content reported for olive pits (64.42%) (Kula et al., 2008), sugar beet bagasse (70-80 %) (Onal et al., 2007) and hazelnut-husk (80.41%) (Karacetin et al., 2014). The other physical properties like bulk density, porosity, and average pore size of prepared activated carbon are given in Table 4.2 which may affect the adsorption capacity. It is seen that the activated carbon prepared from the mango seed kerneal has fairly large surface area and pore size required for a good adsorbent.

Table 4.2 The physical characteristics of the mango kernel activated carbon

Parameters	**Value**
Bulk density (g cm^{-3})	1.43
Porosity	0.576
BET Surface area (m^2 g^{-1})	490.43
Average particle size (µm)	781.5
Average pore size (µm)	38.9
pH at the point of zero surface charge (pHpzc)	6.8

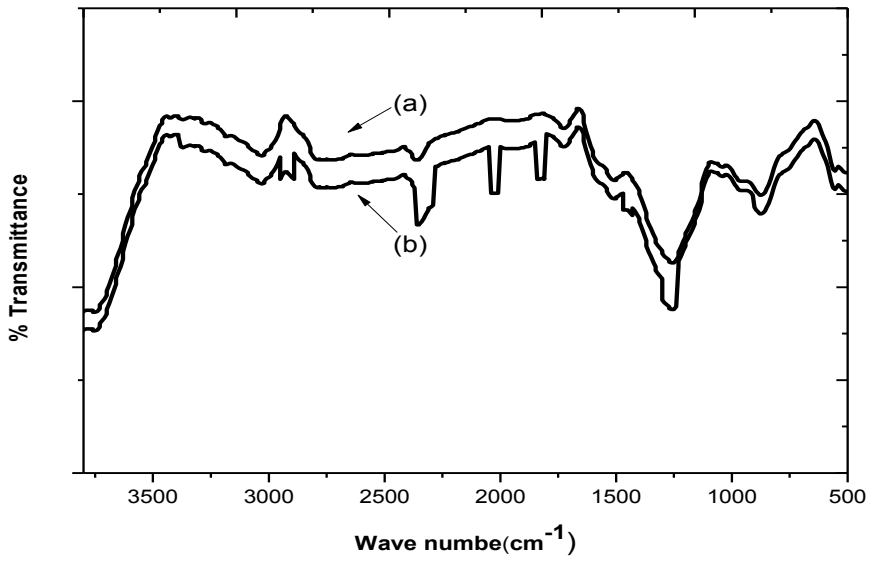

.

Fig. 4.1 FTIR spectra of the MKAC (a) Before adsorption (b) After Cr (VI) loading

The FTIR spectra of the adsorbent before (Fig. 4.1a) and after adsorption (Fig. 4.1b) are recorded. In Fig 4.1(a) the spectrum reveals the complex nature of the adsorbent as evidenced by the presence of a large number of peaks. Absorption peaks around 3030.6 cm^{-1} and 3423.0 cm^{-1}indicate the presence of free and intermolecular bonded hydroxyl groups (Droussi et al., 2009). Peak at 3371.7 cm^{-1} corresponds to N-H stretching showing presence of amines and amide groups (Li et al., 2009). Peaks around 2720.5 cm^{-1} and 1724.3 cm^{-1} can be assigned to the presence of aldehydes, carbonyls, carboxylic acids and esters on the surface (Jain et al., 2010). Peak around 1510.6 cm^{-1} shows presence of nitro compounds on surface (Zhang et al 2010). The peaks around 1254.0 and 876.9 cm^{-1} show the presence of aromatic, amines and hydrocarbons on the surface (Ofomaja et al., 2011). Lastly, peak at 555.5 cm^{-1} shows presence of alkyl halides on surface. These functional groups have a high affinity towards hexavalent chromium. FT-IR spectra of Cr(VI) adsorbed MKAC show low transmittance intensity and the shifted peak locations at different frequencies due to Cr(VI) adsorption (Fig. 4.1b).

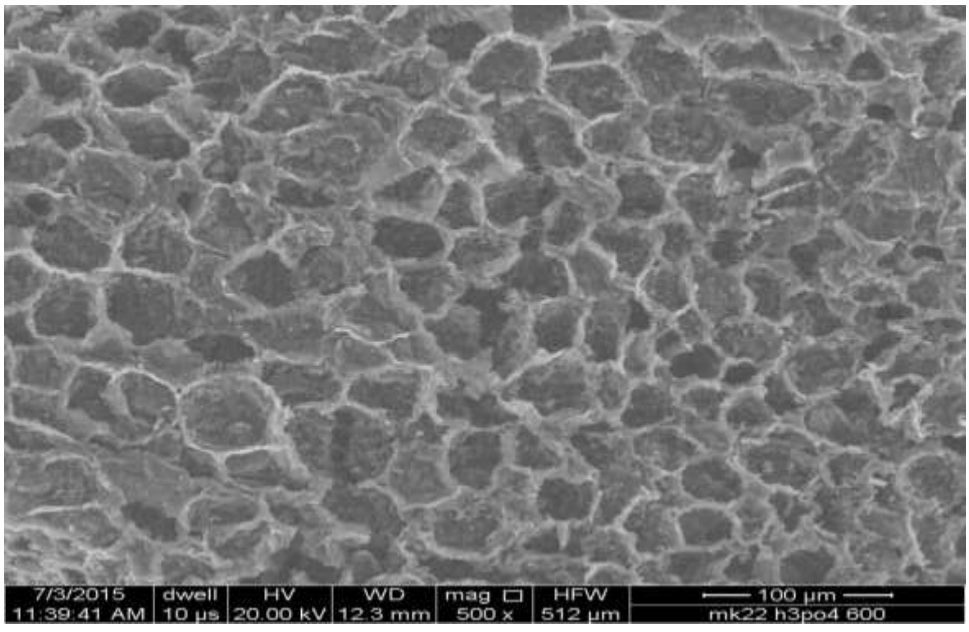

Fig. 4.2 (a) SEM micrograph of MKAC before adsorption

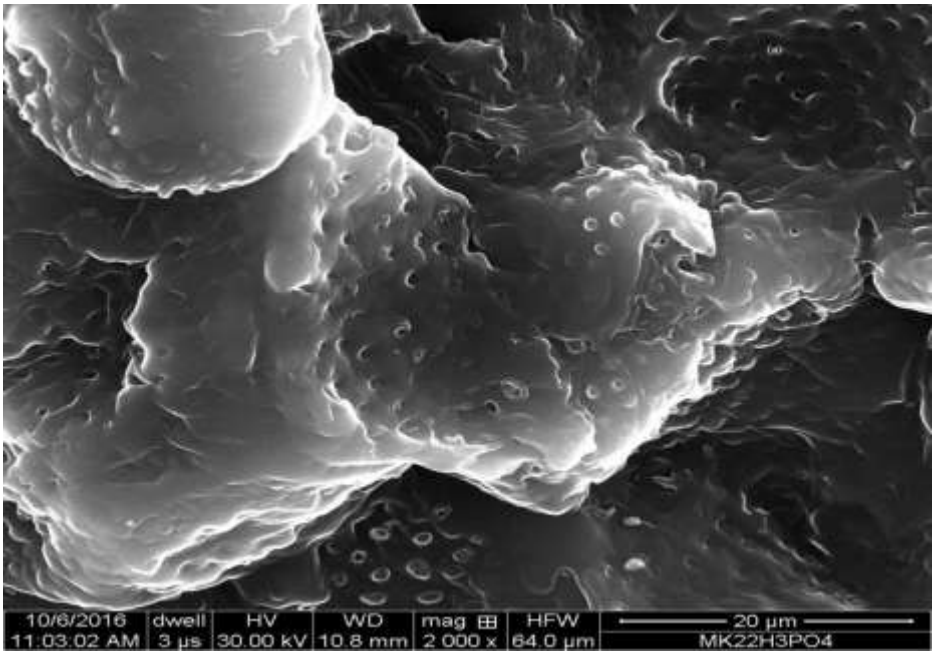

Fig. 4.2 (b) SEM micrograph of MKAC after Cr (VI) adsorption

The SEM micrograph of MKAC before adsorption is shown in Fig. 4.2 (a). It is seen that MKAC has a highly porous structure with greater homogeneity and average pore diameter of 38.9µm. Fig. 4.2 (b) shows the SEM morphology of MKAC after Cr (VI) loading. From the figure it is clear that a layer is formed due to Cr (VI) adsorption on the surface and some Cr(VI) have occupied inside the pores of MKAC.

4.1.2 Effect of solution pH on adsorption

It was found that uptake of Cr (VI) depends on pH and decreases with increasing pH which is shown in Fig. 4.3. The adsorption of metals is related to the surface functional groups and chemistry of the adsorbate metal ion-solvent interaction that vary with the pH. The hexavalent chromium ions can exist as hydrogen chromate ($HCrO_4^-$) or chromate (CrO_4^{2-}) or dichromate ($Cr_2O_7^{2-}$) depending upon the pH of the solution. At acidic pH 2, the dominant form of Cr (VI) is $HCrO_4^-$ and at higher pH other forms CrO_4^{2-} or $Cr_2O_7^{2-}$ predominate. Observed higher adsorption at lower pH can be attributed to the strong electrostatic attraction between positively charged surface

groups and $HCrO_4^-$. Reduced adsorption above pH 6 can be attributed to the competitive adsorption of CrO_4^{2-} and OH^- ions. Earlier worker have also reported similar behavior using other adsorbents (Owlad et al., 2010; Rangabhashiyam and Selvaraju, 2015 (a); Hsua et al., 2009).

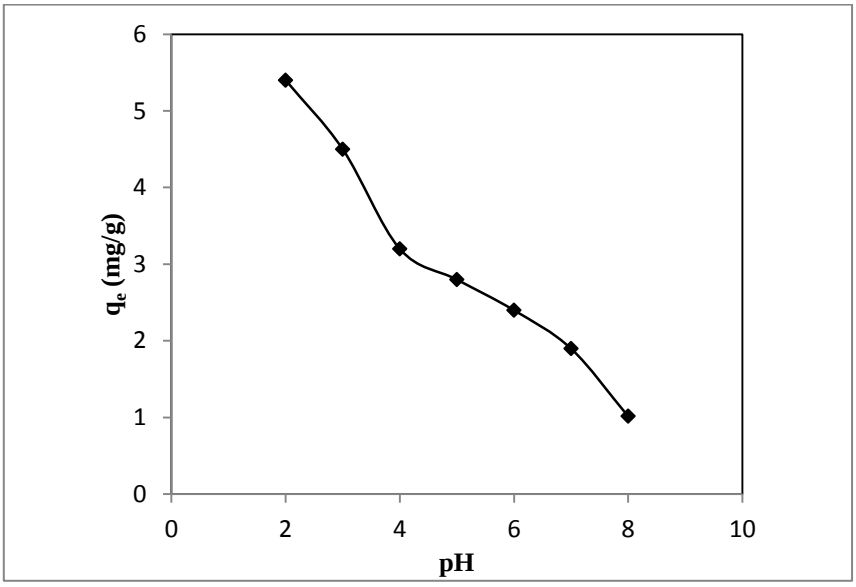

Fig. 4.3 Effect of solution pH on Cr (VI) adsorption by MKAC (Initial concentration: 20 mg/l; Agitation speed: 150 rpm; Dose: 0.25g/100mL; Temperature: 35˚C; time: 190 minute)

4.1.2 Effect of contact time

As shown in Fig. 4.4, the extent adsorption increases steeply with increasing contact time up to around 50 minutes and there after it reduces and tends to a constant value. In the beginning all the active sites on the adsorbent are vacant hence adsorption proceeds at a faster rate and desorption at a lower rate, the net effect is faster increase in the extent of adsorption. As the active sites get occupied, the rate of adsorption and desorption tend to be equal and extent of adsorption reduces and eventually becomes nearly constant at equilibrium. Any further adsorption beyond this is through intra-particle diffusion which is a much slower process (Rangabhashiyam and Selvaraju,

2015 (b), Bayazit and Kerkez, 2014). For the given situation adsorption equilibrium time is observed to be 150 min.

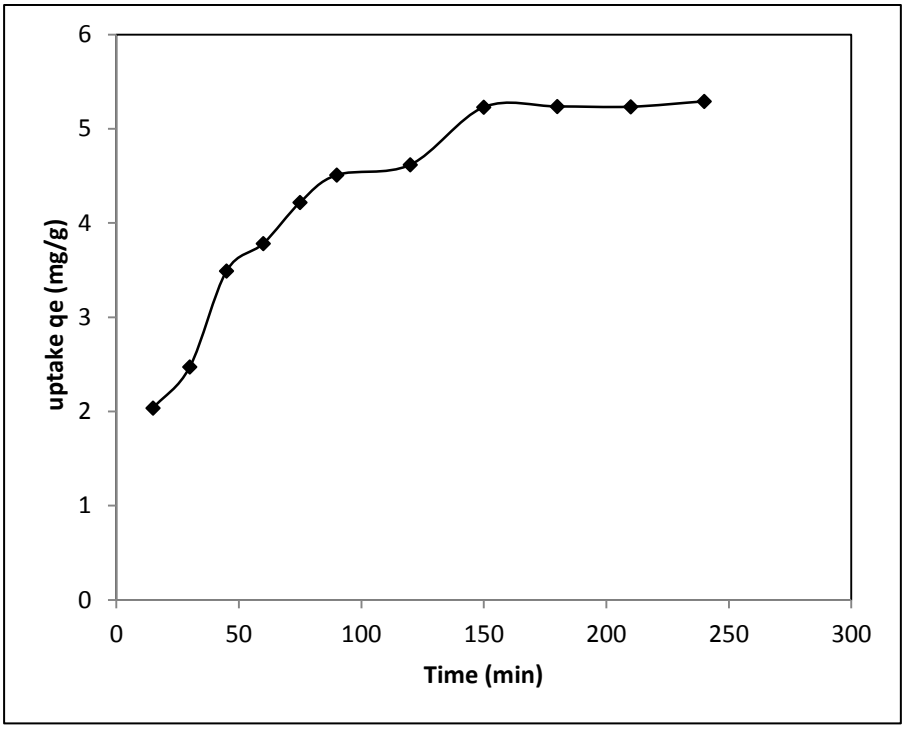

Fig. 4.4 Effect of contact time on Cr (VI) adsorption by MKAC (Initial concentration: 20 mg/l, Solution pH: 2, Agitation speed: 150 rpm, Dose 0.25g/100 mL, Temperature: 35˚C)

4.1.3Effect of adsorption dose

The adsorption results for adsorbent doses of 0.25 g/100 mL to 1.0 g/100 mL are shown in Fig. 4.5. It is seen that the adsorption % has increased from 65 to 100 that can be directly linked to the availability of increasing adsorption sites with increasing amount of adsorbent. At higher adsorbent dose, there are not enough Cr (VI) in the solution to occupy the active sites and hence the adsorption tends to become constant (Jung et al., 2013; Rangabhashiyam and Selvaraju, 2015(c)). In view of this observation, for all other experiments the adsorbent dose was fixed at 0.25 g/100 mL.

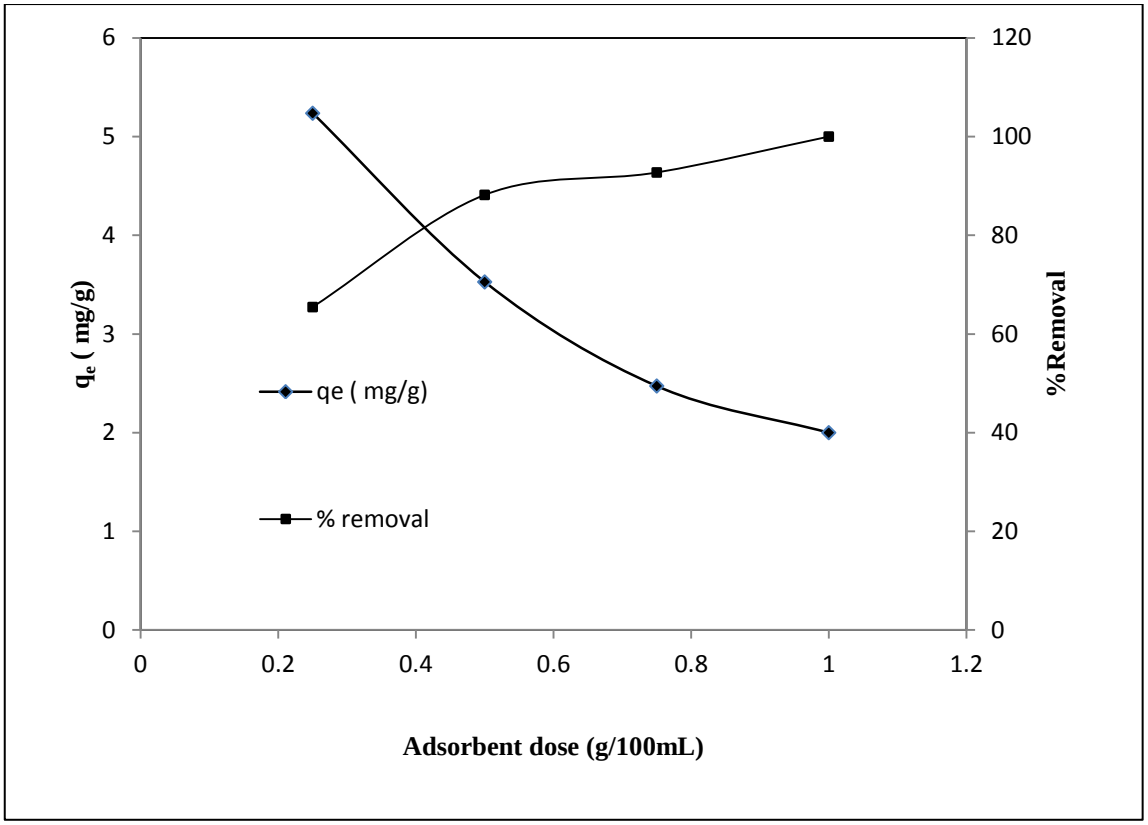

Fig.4.5 Effect of adsorbent dose on metal uptake and percentage metal removal by MKAC (Initial conc.: 20 mg/l; Solution pH: 2; Agitation speed: 150 rpm; Temperature: 35˚C; Contact time: 150 min.)

4.1.4 Effect of initial concentration of Cr (VI)

It can be seen from Fig. 4.6 that in the beginning the Cr (VI) uptake increased with increasing Cr (VI) concentration that gradually reduced at higher concentrations and eventually became constant. After a certain level of increase in initial Cr (VI) concentration, all the active sites on the adsorbent surface get occupied and finally establishing a form of dynamic equilibrium between the processes of adsorption and desorption (Malkoc et al., 2006).

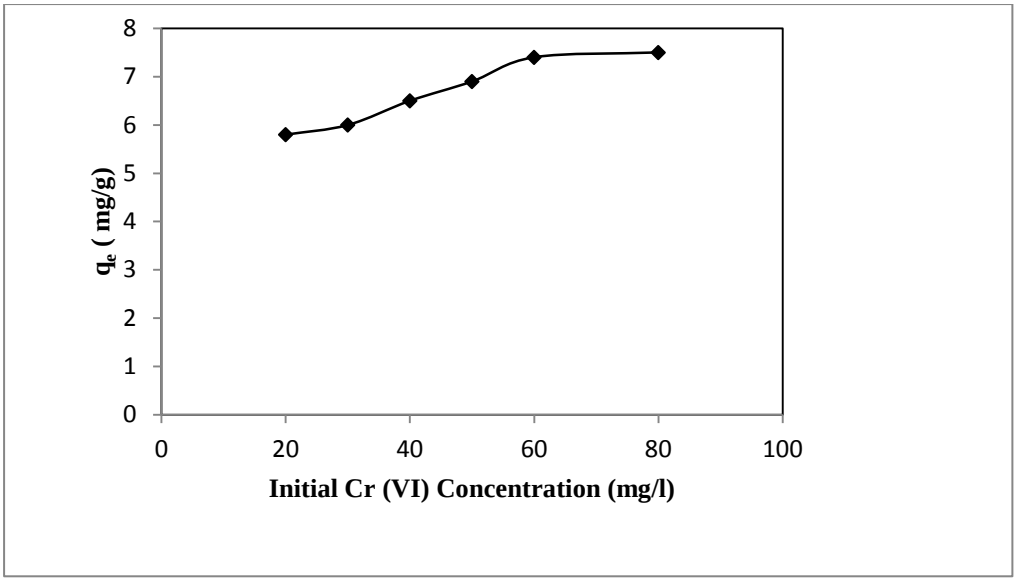

Fig. 4.6 Effect of initial Cr (VI) concentration on metal uptake (mg g^{-1}) by MKAC (Solution pH: 2; Agitation speed: 150 rpm; Dose: 0.75g/100 mL; Temperature 35˚C; Contact time: 150 min.)

4.1.5 Adsorption isotherm study

The equilibrium adsorption data for MKAC were tested with Langmuir (Langmuir, 1918) and Freundlich (Freundlich, 1906), Tempkin and Dubinin- Radushkevich modes to know which isotherm is better suited for Cr (VI) removal. All the parameters of these isotherms were presented in Table 4.3. A further analysis of Langmuir isotherm can be made using the dimensionless equilibrium parameter R_L which is presented in Table 4.3. The value of R_L lies between 0 and 1 for a favourable adsorption, while $R_L > 1$ represents an unfavourable adsorption, for $R_L = 1$ adsorption is linear and if $R_L = 0$, it is irreversible. The dimensionless parameter, R_L is found in the range of 0 to 1, which confirms the favorable adsorption process for Cr (VI) removal. The Freundlich constants, K_f and n cab are calculated by plotting the graph between $ln\ q_e$ versus $ln\ C_e$ as shown in Fig. 4.8. The adsorption isotherm parameters of the all isotherms are shown in Table 4.3. Langmuir equation is shown as C_e/q_e versus C_e plot in Fig. 4.7. The values of q_m are obtained as 7.5, 7.8 and 7.9 mg g^{-1} at the temperature of 25, 30 and 35 ^{0}C,

respectively. The coefficient of correlation for Freundlich isotherm model is much lower than that of Langmuir isotherm model as given in Table 4.3.

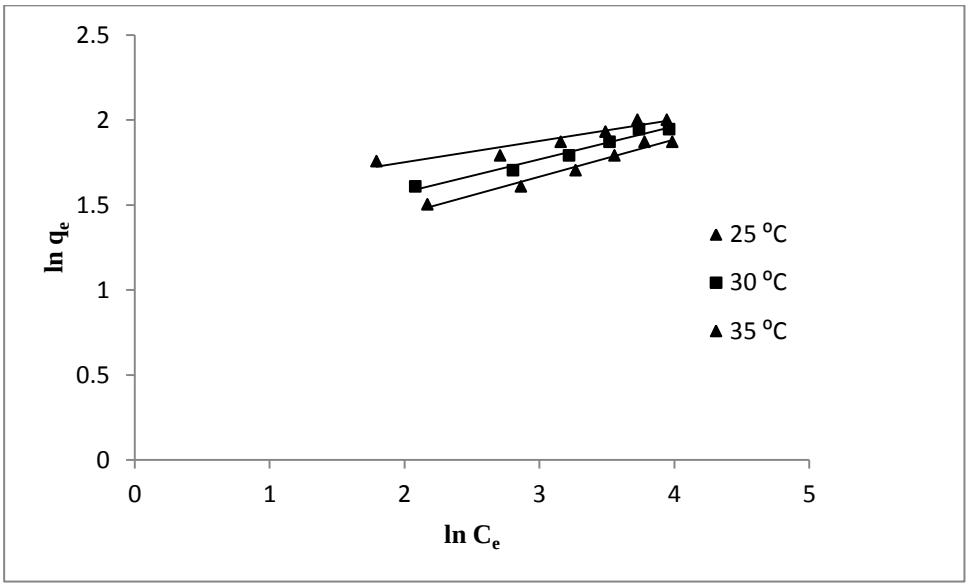

Fig. 4.7 Langmuir isotherm model for the Cr (VI) adsorption onto MKAC (Solution pH: 2; Agitation speed: 150 rpm; Dose: 0.25g/100 mL; Time: 150 min.)

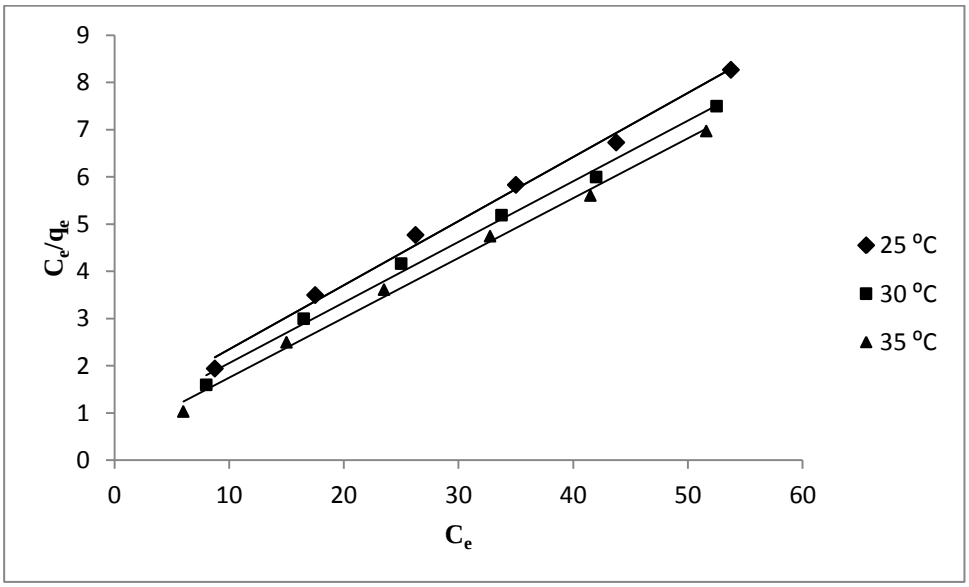

Fig. 4.8 Freundlich isotherm model for the Cr (VI) adsorption onto MKAC (Solution pH: 2; Agitation speed: 150 rpm; Dose: 0.25g/100 mL; Time: 150 min.)

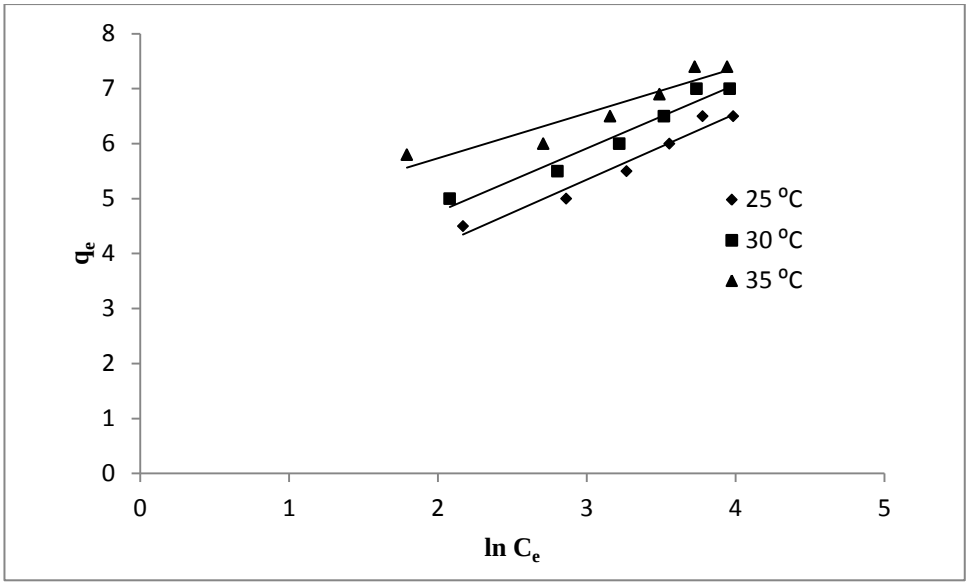

Fig. 4.9 Tempkin isotherm model for the Cr (VI) adsorption onto MKAC (Solution pH: 2; Agitation speed: 150 rpm; Dose: 0.25g/100 mL; Time: 150 min.)

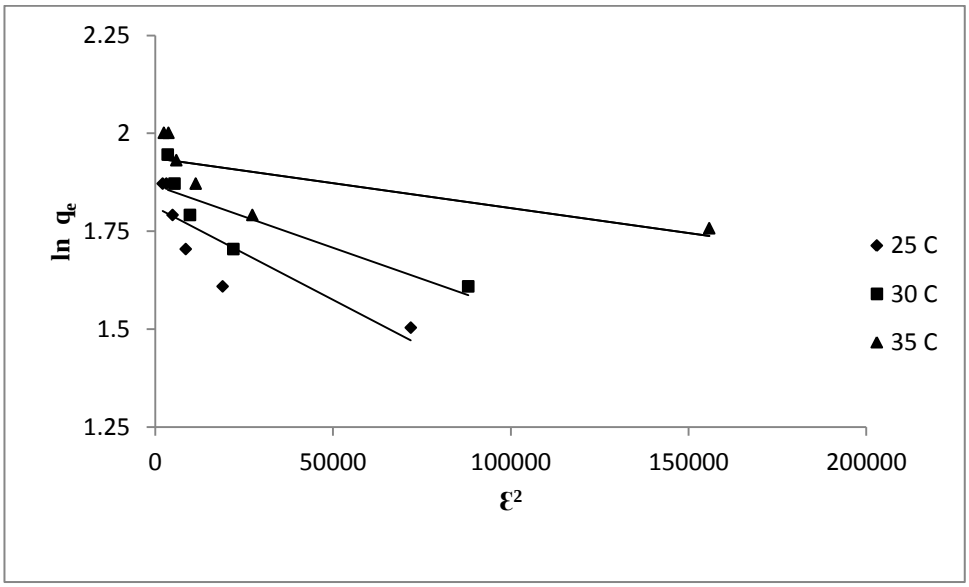

Fig. 4.10 D-R isotherm model for the Cr (VI) adsorption onto MKAC (Solution pH: 2; Agitation speed: 150 rpm; Dose: 0.25g/100 mL; Time: 150 min.)

The parameters of Tempkin isotherm were observed by graph between q_e verses $ln\ C_e$ at different temperatures of 298, 303 and 308 K. The calculated data of A_T and b_T were presented in Table 4.3.The correlation coefficient R^2 is found as

0.9602, 0.9579 and 0.8897 at different temperatures which is lower in compression to Langmuir isotherm. The parameters of Dubinin-Radushkevich were also calculated by the plot of $ln\ q_e$ verses $\mathcal{E}^2$ at different temperature. The value of q_m, E and K are calculated by this graph. The value of E (0.707 KJ/mol) is less than 16KJ/mol, which revels the physical adsorption rather than chemical adsorption. The coefficient of correlation is found as 0.7398, 0.7261 and 0.5461, which are much lower than other isotherm. After overall compression of data the Langmuir isotherm is fitted best for adsorption of Cr (VI) on MKAC.

Table 4.3 Adsorption isotherm parameters for Cr (VI) removal using MKAC

Adsorption isotheres	**Parameters**	**Temperature**		
		25 ^{0}C	30 ^{0}C	35 ^{0}C
Langmuir isotherm	q_m	7.42	7.83	7.96
	b	0.135	0.166	0.2634
	R^2	0.993	0.994	0.995
	R_L	0.2702	0.2312	0.157
Freundlich isotherm	K_f	1.24	1.21	1.198
	n	0.99	0.84	0.76
	R^2	0.974	0.971	0.974
Tempkin	A_T	4.30	8.20	147.82
	b_T	2067.3	2175	3123.58
	R^2	0.9602	0.9579	0.8897
Dubinin-Radushkevich	q_m	3.25	6.60	6.9303
	$K\times10^6$	5.01	3.02	1.02
	E	0.3159	0.407	0.707
	R^2	0.7398	0.7261	0.5461

4.1.6 Kinetic study

The kinetic data was analyzed for three kinetic models such as the pseudo-first order, pseudo-second order and intra particle diffusion model. The pseudo-first order kinetic model is presented in Fig. 4.11 as $ln(q_e - q_t)$ verses t (min) at different initial concentration of Cr (VI) such as 20, 30, and 40 mg/l. The coefficient of correlations was found as 0.961, 0.957 and 0.965 which are compared with other kinetic model. The parameters of intra- particle diffusion model are tabulated in Table 4.4, which reveals that the increase in boundary layer thickness because the value of I is increasing with increased initial concentration of Cr (VI). The value of I is greater than zero which suggests the other kinetic model is also involved other than intra particle diffusion mode. The q_e value calculated from the experiment is nearly equal to calculated value of q_e from pseudo- second order model. The value of R^2 was compared for all three kinetic models and it was found, maximum for pseudo second order model, having values of 0.985, 0.984 and 0.981 at different initial concentration of Cr (VI).

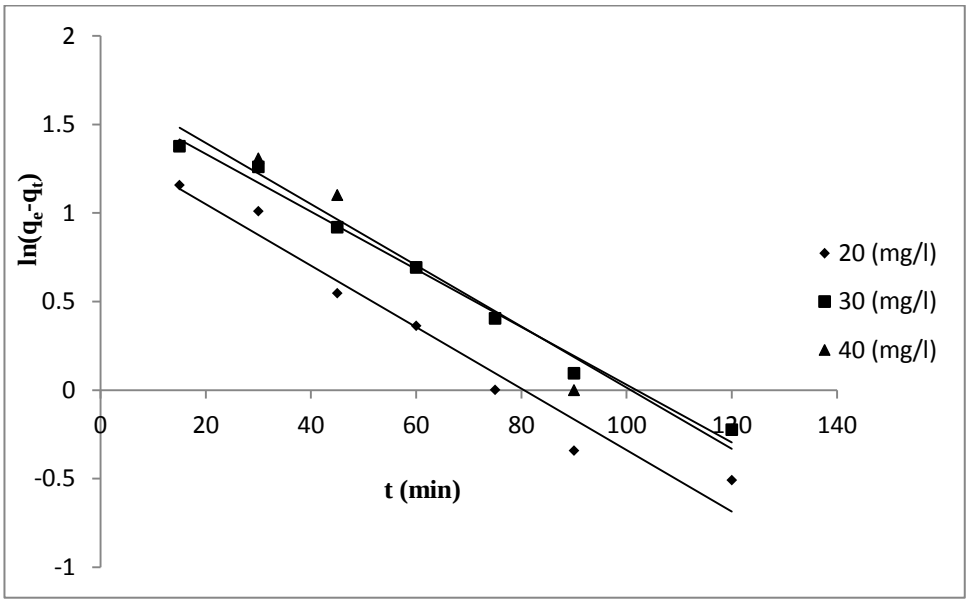

Fig. 4.11 Pseudo-first-order kinetic model for removal of Cr (VI) by MKAC (Solution pH: 2; Dose: 0.25g/100 ml, Agitation speed: 180 rpm; Temperature 35 ^{0}C).

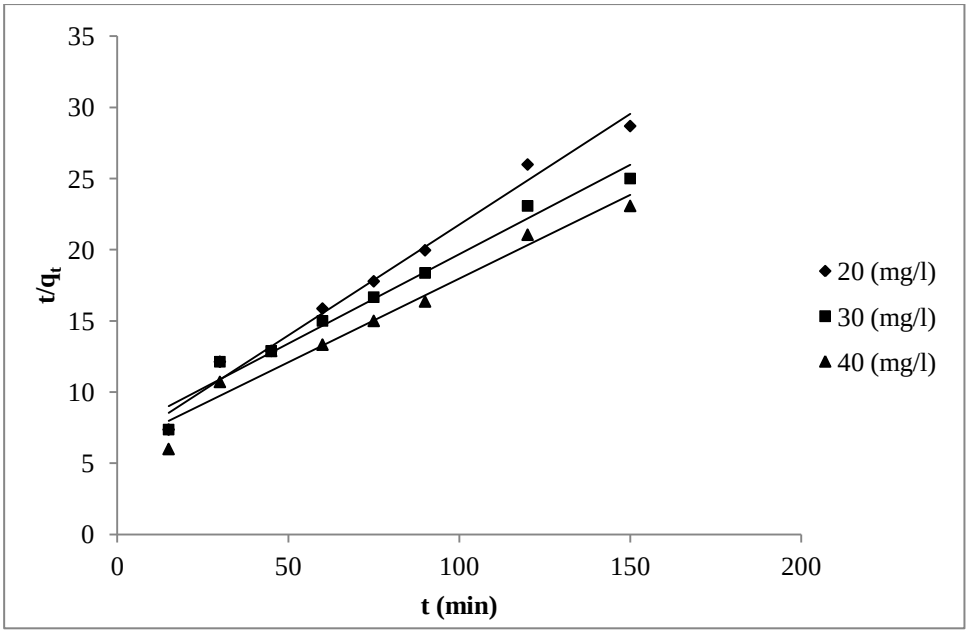

Fig. 4.12 Pseudo-second-order kinetic model for removal of Cr (VI) by MKAC (Solution pH: 2; Dose: 0..25g/100 mL, Agitation speed: 180 rpm; Temperature 35 ^{0}C).

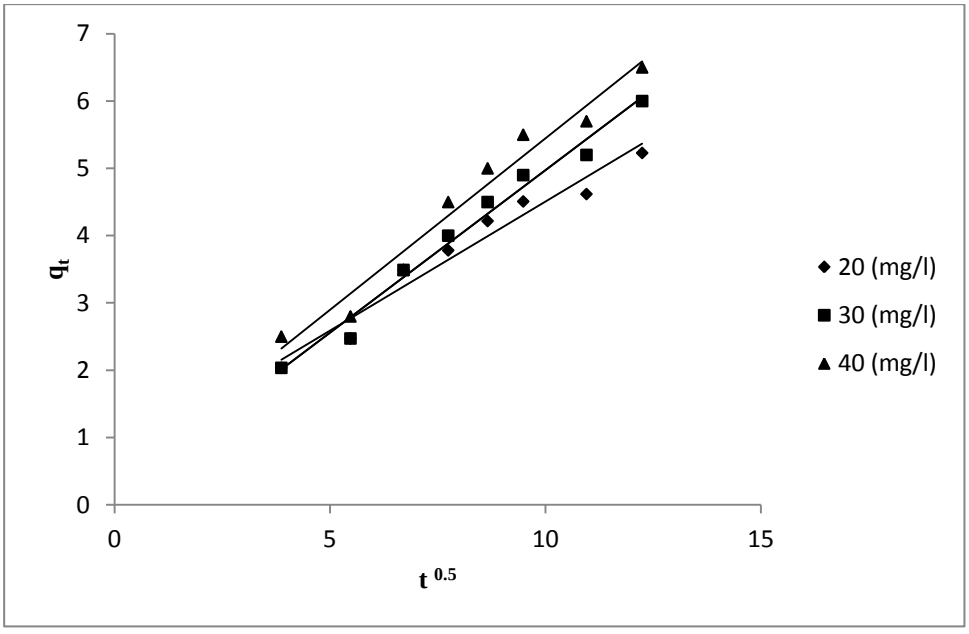

Fig. 4.13 Intra particle diffusion model for removal of Cr (VI) by MKAC (Solution pH: 2; Dose: 0..25g/100 mL, Agitation speed: 180 rpm; Temperature 35 ^{0}C).

Table 4.4 Kinetic parameters for the adsorption of Cr (VI) on MKAC at different initial concentration

Kinetic parameters models	Initial concentration (mg/L)		
	20	30	40
q_e(exp) (mg/g)			
Pseudo- first- order model			
k_1	0.017	0.016	0.017
q_e(cal)	4.04	5.25	5.60
R^2	0.961	0.957	0.965
Pseudo -second -order model			
$k_{2\times 10^{-3}}$	3.87	2.19	2.21
q_e(cal)	6.45	8.01	8.54
R^2	0.985	0.984	0.981
Intra- particle diffusion model			
k_{id}	0.3835	0.4825	0.5095
I	0.672	0.1457	0.349
R^2	0.957	0.981	0.966

4.1.7 Thermo dynamic study

The feasibility of adsorption of Cr (VI) on the surface of MKAC was carried out by thermodynamic study at different temperature such as 298, 303 and 308 K. For calculation of these thermodynamic parameters such as Gibbs free energy (ΔG°), enthalpy change (ΔH°) and entropy change (ΔS°) are observed at the optimum condition of adsorption. From the Fig. 4.14, the values of these thermodynamic were evaluated and the parameters are presented in Table 4.5. The values of Gibbs free energy were calculated as -15.603, -16.219 and -17.60 at temperatures of 298, 303 and 308 K, respectively. The negative value of Gibbs free energy shows the spontaneous nature of the adsorption of Cr (VI) on MKAC. The positive value of entropy change ($\Delta H^\circ = 43.76$ KJ/mol) confirmed the endothermic nature of adsorption process of Cr

(VI). Also the positive value of (ΔS°=198.80J/mol K) indicated the increase in randomness with increasing temperature for the adsorption of Cr (VI) on MKAC.

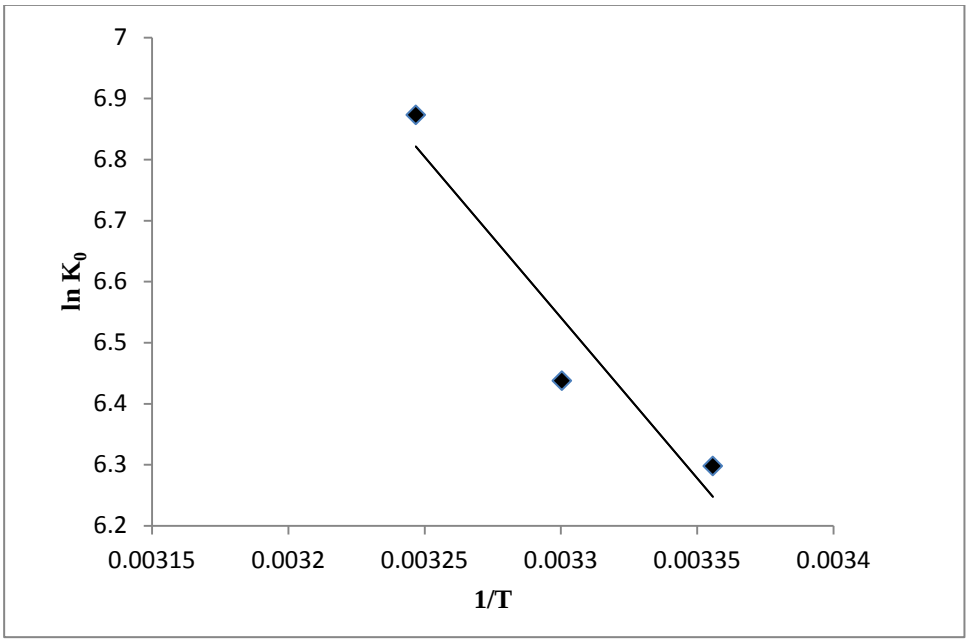

Fig. 4.14 Determination of thermodynamic properties for adsorption of Cr(VI) on MKAC

Table 4.5 Thermodynamic parameters for the adsorption of Cr (VI) on MKAC

Temperature(K)	ΔG° (KJ/mol)	ΔH° (KJ/mol)	ΔS° (J/molK)
298	-15.603		
303	-16.219	43.76	198.80
308	-17.60		

4.1.8 Conclusions

Activated carbon from mango (*Mangiferaindica*) seed kernel was prepared with H_3PO_4 activation carbonized at 600 °C. The characterization results was shown that the high surface area (490.43 m^2/g) and porosity. The FTIR spectra of activated carbon revealed different functional groups which was useful in adsorption. Its adsorption efficacy was tested for removal of Cr (VI) from aqueous solution. The adsorption of Cr (VI) was found to be strongly dependent on pH, adsorbent dose, contact time and initial Cr (VI) concentration. The pH 2.0, adsorbent dose of 2.5g/100 mL and equilibrium time of 150 min were found to be the optimum conditions for the maximum Cr (VI) uptake of 7.8 mg g^{-1}. Langmuir isotherm fitted the equilibrium data well. The pseudo- second order model explained the kinetic data well. The positive value of entropy change (ΔH° = 43.76 KJ/mol) confirmed the endothermic nature of adsorption process of Cr (VI).

Section -B

4.2 Adsorption of chromium Cr (VI) by almond shell activated carbon (ASAC1)

In this part adsorption of Cr (VI) from aqueous phase by activated carbon prepared from almond shell. The effect of different operating parameters such as effect of initial pH of Cr(VI) solution, initial concentration of Cr(VI) solution, contact time, dose of almond shell activated carbon and temperature have been determined the study of the adsorption isotherms and kinetics models.

4.2.1 Characterization of activated carbon

The pH_{pzc} value of ASAC1 was found to be 5.5, which indicates that at this pH the net surface charge of the activated carbon is zero, whereas at pH <5.5, the adsorbent surface is positively charged and at pH >5.5, it is negatively charged.

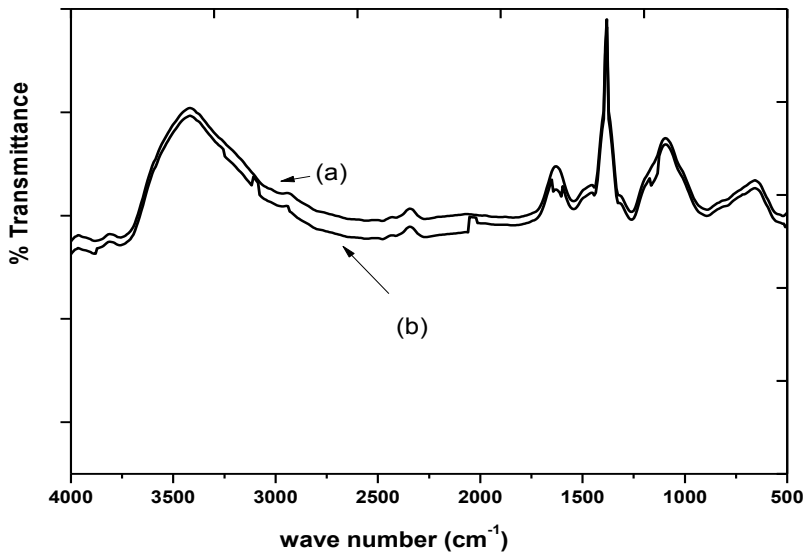

Fig. 4.15 FTIR spectra of the almond shell activated carbon (a) Before adsorption (b) After Cr (VI) loading

The FTIR spectra of the almond shell activated carbon before and after adsorption were recorded in the range of 400–4000 cm^{-1}. The peaks at wave numbers of 650 cm^{-1} indicate the C–H vibration of the aromatic compounds; the peak at 1590 and 1385 cm^{-1} correspond to -COO- and >C=O- groups, that at 1820–1900 cm^{-1} correspond to the >C=O- stretch of saturated carboxylic acids and aliphatic esters (Droussi et al., 2009;Zhang et al., 2011; Chia et al., 2012; Singh et al., 2017; Talha et al. 2018).The peaks around 2760.5–1899.5 cm^{-1}might be assigned to aldehydes, carbonyls, carboxylic acids and esters present on the surface (Pedroza et al., 2014; Kanjurang et al., 2017; Talha et al., 2018).These functional groups have an affinity toward chromium ions. FTIR spectra of Cr(VI) loaded ASAC show the shifted peak locations and low transmittance intensity at 3428, 2934, 1634 and 1246 cm^{-1} due to Cr(VI) adsorption (Fig. 4.15).

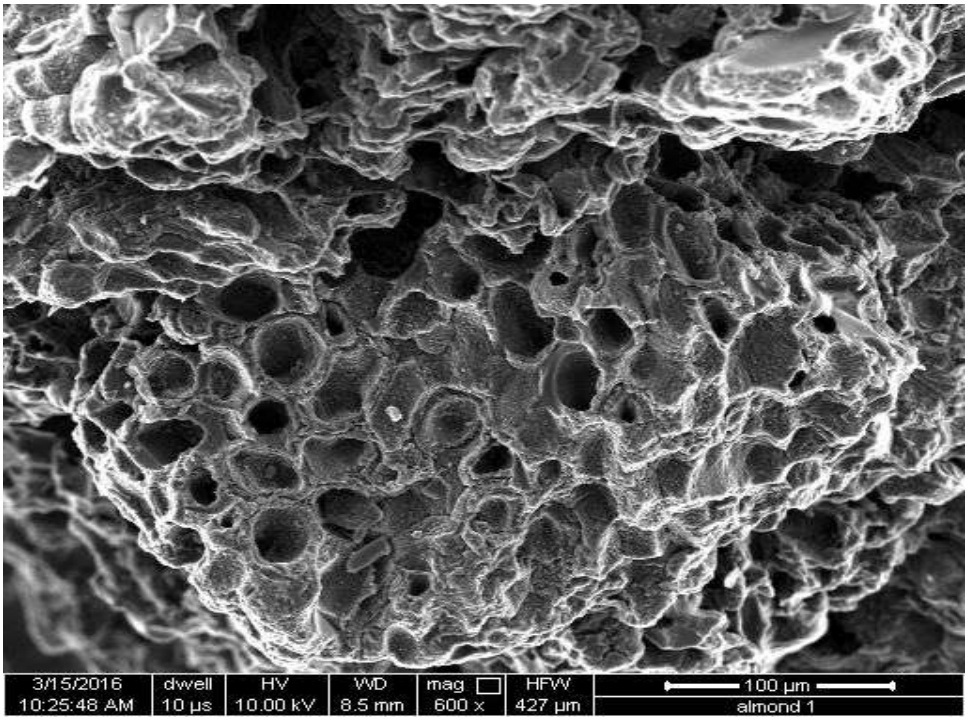

Fig. 4.16 (a) SEM micrograph almond shell activated carbon before adsorption of Cr(VI)

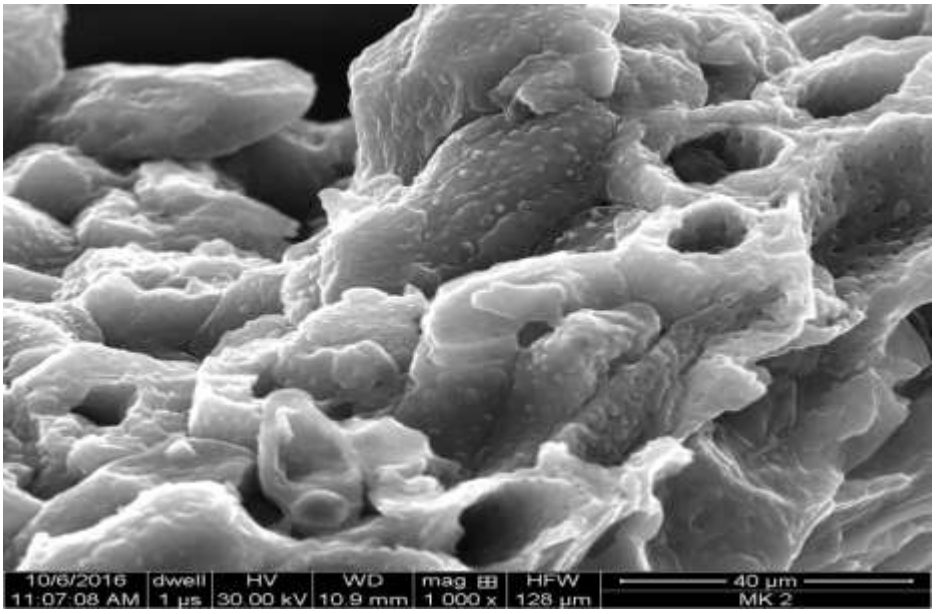

Fig. 4.16 (b) SEM micrograph almond shell activated carbon after adsorption of Cr(VI)

Differences in SEM images were observed between surface topography of ASAC1 before and after adsorption. SEM photomicrographs before and after adsorption are shown in Fig. 4.16. From Fig. 4.16, it is clear that ASAC1 has a highly porous structure with greater homogeneity. The SEM photomicrograph after Cr (VI) adsorption shows that a layer is formed due to Cr (VI) adsorption on the surface of the activated carbon and some Cr (VI) has also filled the pores.

From Table 4.6, it is observed, as expected, that the percent carbon content in activated carbon (78.0%) is substantially higher than that of raw almond shell (44.4%). This is nearly comparable to other activated carbon reported for olive pits (64.4%) (Ugurlu and Karaoglu, 2008), sugar beet bagasse (70–80%) (Onal et al., 2007) and hazelnut-husk (80.4%) (Karacetin et al., 2014).The Brunauer–Emmett–Teller (BET) surface area of the adsorbent was found to be 1223 m^2/g which indicates that ASAC1 may be a good adsorbent for adsorption of Cr (VI) and other pollutants from wastewater (Table 4.6). The other important physical properties like pore volume, average pore size

and point of zero charge of prepared activated carbon were found to be 0.3266 cm^3/g, 2.39 nm and 5.20 (Table 4.6), respectively, which may play an important role in the adsorption.

Table 4.6 Physical properties of almond shell activated carbon

Parameters	**Value**
BET Surface area ($m^2\ g^{-1}$)	1223
Pore volume ($cm^3\ g^{-1}$)	0.326563
Average pore size (nm)	2.39
pH at the point of zero surface charge (pHpzc)	5.2
Elemental analysis (%)	
C	75.56
H	2.55
N	1.45
S	0
O	15.44

4.2.2 Effect of various parameter for Cr (VI) adsorption

4.2.2.1 Effect of adsorbent dose and contact time

From Fig. 4.17, it is observed that the removal of Cr(VI) is rapid in the early stages up to 100 minutes and becomes almost constant after 240 minutes. This may be due to the availability of more adsorption sites for the removal of Cr(VI) ions at the initial stage, and after some time the slow rate of Cr(VI) adsorption is due to hindrance or repulsion of absorbed Cr(VI) ions onto the adsorbent surface (Husa et al., 2009). Due to this, the graph is tapered after 150 minutes. It is observed that the uptake of Cr(VI)

increases as amount of the adsorbent dose decreases. From Fig. 4.17, it is clear that the adsorption capacities decreased from 16 to 4mg/g as the dosage was increased from 2.5 to 10 g/L. Fig. 4.17 shows that the increasing the adsorbent doses above the optimum value, do not result in an increase in the Cr (VI) ion uptake .This can be explained by the overlapped and unsaturated sites of the adsorbent. In initial stage of adsorption more active sites are present which have capability to attract the hexavalent chromium on the surface but after some time these active sites being filled by Cr(VI), shows less adsorption capacity.

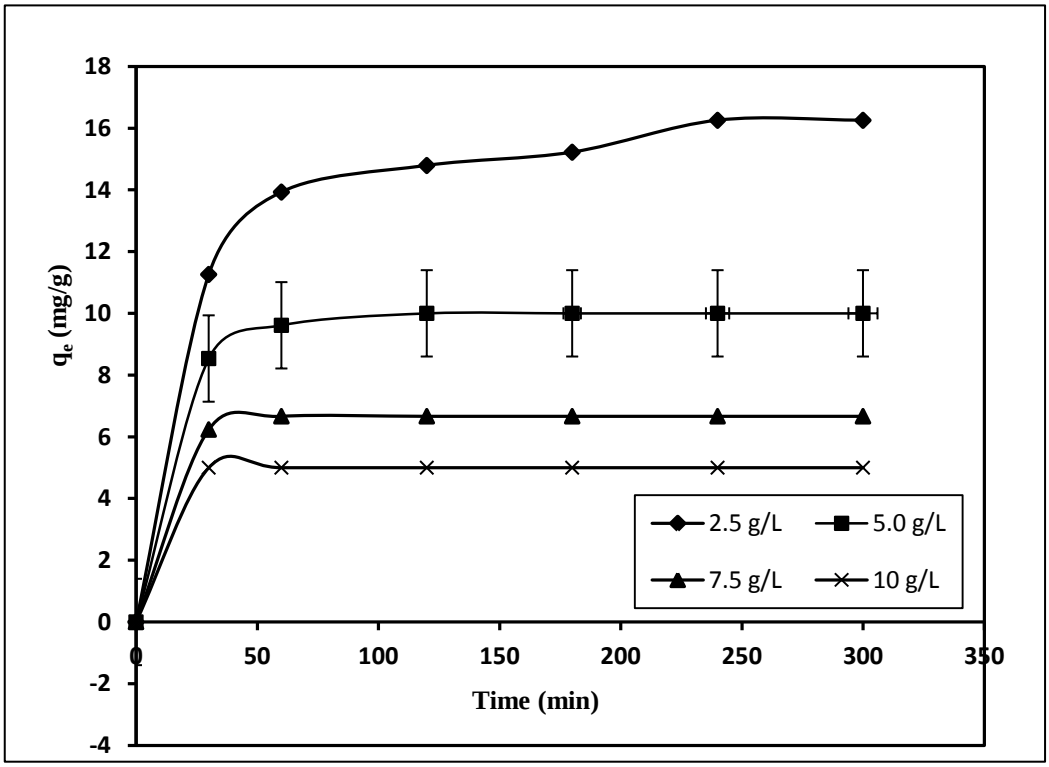

Fig. 4.17 Effect of activated carbon dose and contact time on metal uptake **(**Initial concentration: 50 ppm, pH: 6, Agitation speed: 150 rpm, Temperature: 35˚C)

4.2.2.2 Effect of pH

Figure 4.18 exhibits the influence of pH (2–8) on the adsorption process. As seen from Figure 4.18, the uptake of Cr (VI) from aqueous solution is dependent on the pH value, and the maximum adsorption capacity is found to be 20 mg/g at pH 2.0. Increasing the pH values from 2.0 to 8.0, results in decrease in the Cr (VI) adsorption capacity. This could be explained by the fact that Cr(VI) exists in ionic form and the existence of these ions, such as $CrO_4^{2-,}$ $HCrO_4^-$ or $Cr_2O_7^{2-}$, depend on the pH of the aqueous solution (Suksabye and Thiravetyan, 2012).Within the pH range of 2.0–6.0, $HCrO_4^-$ and $Cr_2O_7^{2-}$ ions are found in equilibrium, and after increasing the pH chromate ions (CrO_4^{2-}) predominate. The chromate ion (CrO_4^{2-}) needs two active sites due to its two minus charges, $HCrO_4^-$ or $Cr_2O_7^{2-}$ ions only need one active site where as a chromate ion (CrO_4^{2-}) needs two active sites due to its two negative charges.

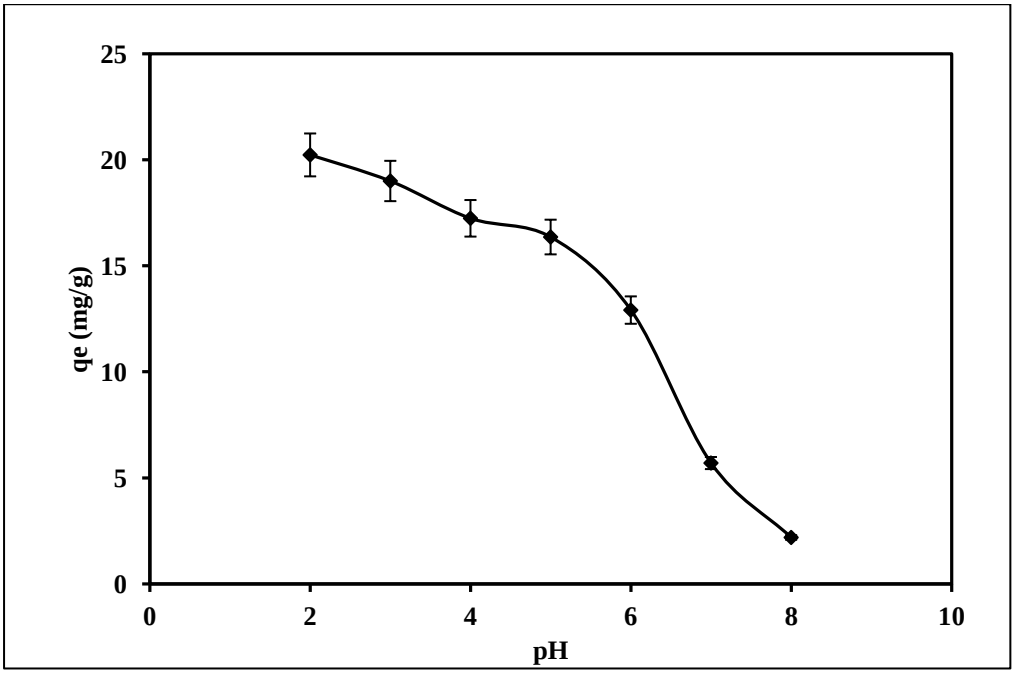

Fig. 4.18 Effect of pH on metal uptake by almond shell activated carbon (Initial concentration: 50 mg/L, Time: 240 min, Agitation speed: 150 rpm, Temperature: 35˚C, Dose: 2.5g/L)

Hence, an increase in the adsorption capacity of Cr (VI) is observed due to more $HCrO_4^-$ ions at lower pH values which need a single site for adsorption (Baral et al., 2006). At higher pH the adsorption capacity is decreased due to competitive adsorption between chromate and hydroxyl ions. The surface of the adsorbent was positively charged at a pH lower than the pH_{pzc} and negatively charged at pH values greater than pH_{pzc}. Thus, the initial solution pH of 2.0 was selected as the optimum pH value for Cr (VI) adsorption for all the remaining experiments.

4.2.2.3 Effect of initial Cr (VI) concentration

The effect of initial concentration on Cr (VI) removal by ASAC1 was studied at different initial Cr (VI) concentrations (100–1000 mg/L) at a contact time of 240 min, pH of 2 and optimal adsorbent dosage of 2.50 g/L. The adsorption capacity increased from 40.0 to 168 mg/g as initial Cr(VI) concentration increased from 100 to 1000 mg/L(Fig. 4. 19). Statistical analyses of findings were carried out using basic statistical software.

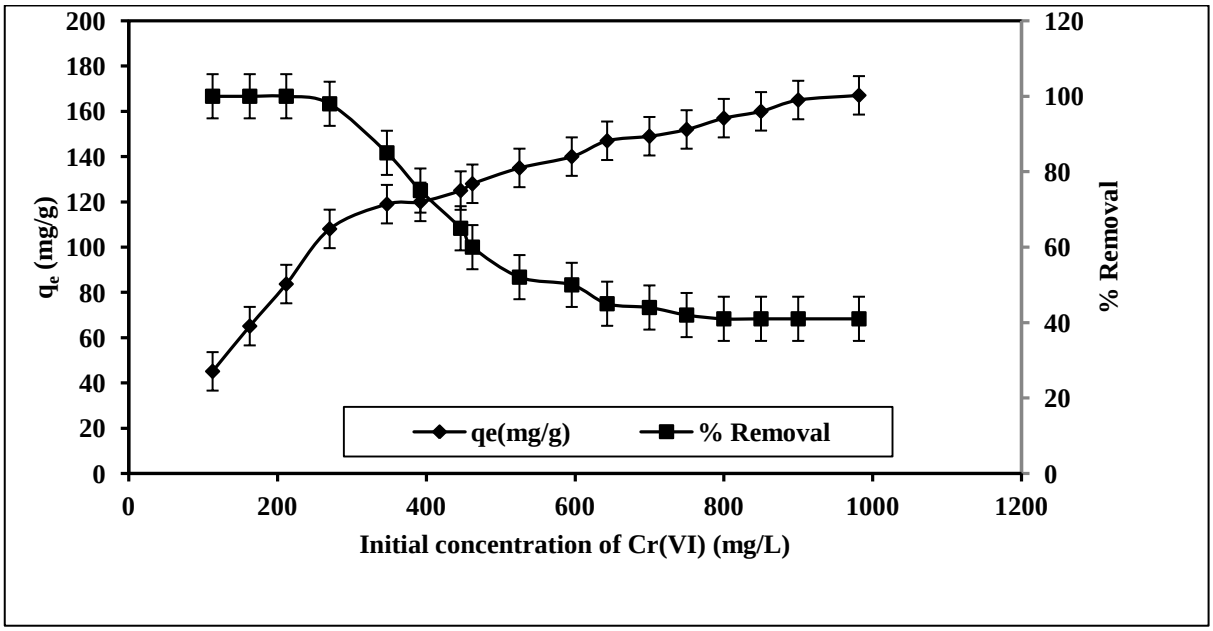

Fig. 4.19 Effect of initial concentration of Cr (VI) on metal uptake and % removal by almond shell activated carbon at (pH 2; Time 4 h; Agitation sped 150 rpm; Temperature 35˚C; Dose 2.5 g/L).

Standard deviation was found to be 26.2 and relative standard error was10.6 for removal efficiencies. The increase in adsorption capacity of the adsorbents with an increase in initial Cr (VI) concentration is due to more interaction of Cr (VI) ions with the absorbent surface (Verma et al., 2006; Nemar, 2009). The percentage removal of Cr (VI) decreased from 100 to 40.5% with increase in Cr(VI) concentration from 100 to 1000 mg/L. The decrease in percentage removal of Cr (VI) is due to less active sites being available for Cr (VI) ions because their sites saturate above a certain concentration. Therefore, Cr (VI) removal was dependent on initial Cr (VI) concentration.

4.2.3 Adsorption isotherm

The values of the adsorption isotherm parameters and the coefficient of determination (R^2) of four equilibrium models at different temperatures are shown in Table 4.7.The maximum adsorption capacities (q_m) determined by the Langmuir model were found to be 202.34, 197.34 and 195.34 mg/g at temperatures of 35, 30 and 25ºC, respectively. The coefficient of determination values (R^2) were found to be high for the Langmuir model in comparison to the other three models which confirmed the monolayer adsorption of Cr (VI) on ASAC1. The calculated R_L values were in the range 0–1 which indicated favorable adsorption of Cr (VI). Freundlich parameters were determined from the linear plot of ln (q_e) versus ln (C_e). The obtained n values were greater than 1.0, which indicated a favorable Cr(VI) adsorption process. The R^2 values for the Freundlich model were very low as compared to the Langmuir model, which suggests that equilibrium data do not follow the Freundlich isotherm model.

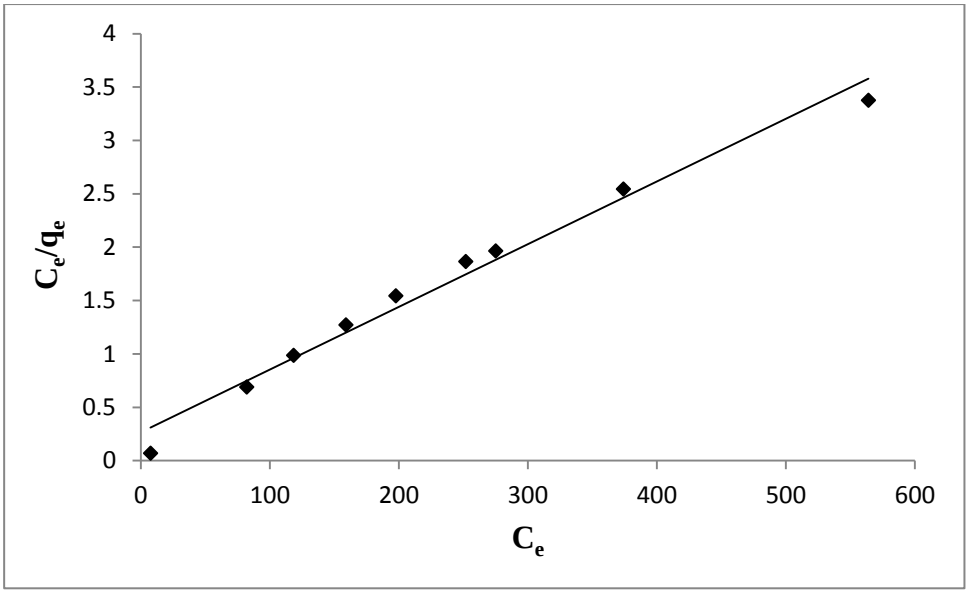

Fig. 4.20 Langmuir isotherm for removal of Cr (VI) (Solution pH: 2; Dose: 2.5 g/100 ml; Agitation speed: 150 rpm; Temperature: 35 ^{0}C)

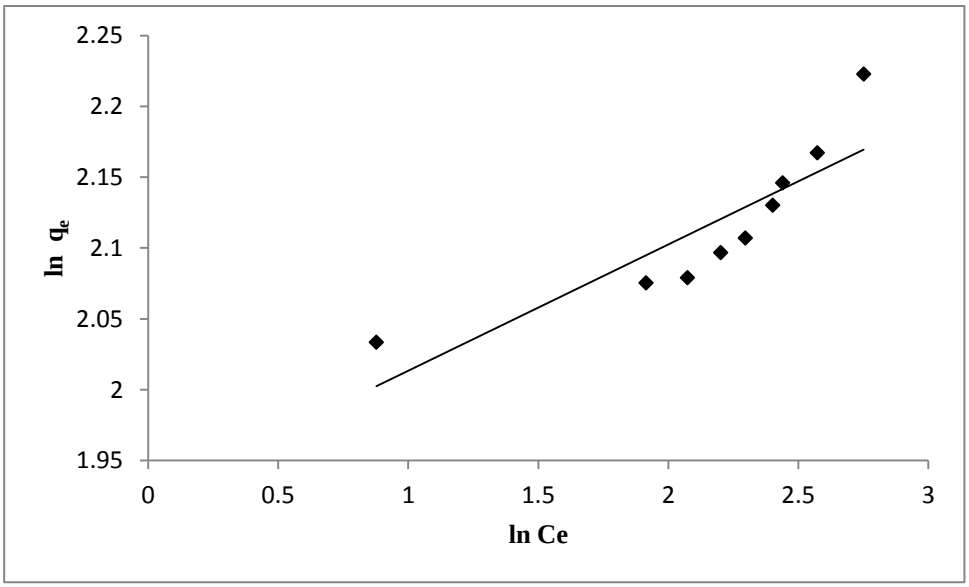

Fig. 4.21 Freundlich isotherm for removal of Cr (VI) (Solution pH 2; Dose 2.5 g/100 ml; Agitation speed 150 rpm; Temperature 35 ^{0}C)

The constants A_T and b_T, were obtained for the Temkin isotherm model and are tabulated in Table 4.7. The R^2 value for the Temkin isotherm is 0.712 which is less than that for the Langmuir isotherm model. The constants, q_m and K obtained for the Dubinin–Radushkevich isotherm model were 134.42 mg/g and 2.0×10^{-6} mol^2/J^2,

respectively at 35 ºC. The maximum absorption capacity, q_m, obtained using the D–R model was 134.42 mg/g which is less in comparison to the Langmuir model (202.34 mg/g). The mean free energy of adsorption (E) was obtained as 0.5 kJ/mol at 35 ºC, i.e. lower than 8.0 kJ/mol. This indicates that the adsorption mechanism is governed by physical adsorption. The value of the coefficient of determination (R^2=0.784) obtained for the D–R model is significantly lower than that of the Langmuir model (R^2=0.987).

Table 4.7 Isotherm parameters for Cr (VI) adsorption on ASAC1

Adsorption isotheres	**Parameters**	**Temperature**		
		25 ^{0}C	30 ^{0}C	35 ^{0}C
Langmuir isotherm	q_m	195.34	197.34	202.34
	b	0.024	0.027	0.018
	R^2	0.976	0.964	0.986
	R_L	0.4545	0.4255	0.5263
Freundlich isotherm	K_f	79.35	80.74	84.34
	n	1.334	1.247	1.124
	R^2	0.8945	0.835	0.876
Tempkin	A_T	862.64	701.345	627.63
	b_T	226.67	223.32	220.18
	R^2	0.643	0.661	0.712
Dubinin-Radushkevich	q_m	132.55	133.54	134.42
	$K\times10^6$	3.02	2.50	2
	E	0.4068	0.447	0.5
	R^2	0.7532	0.7732	0.7854

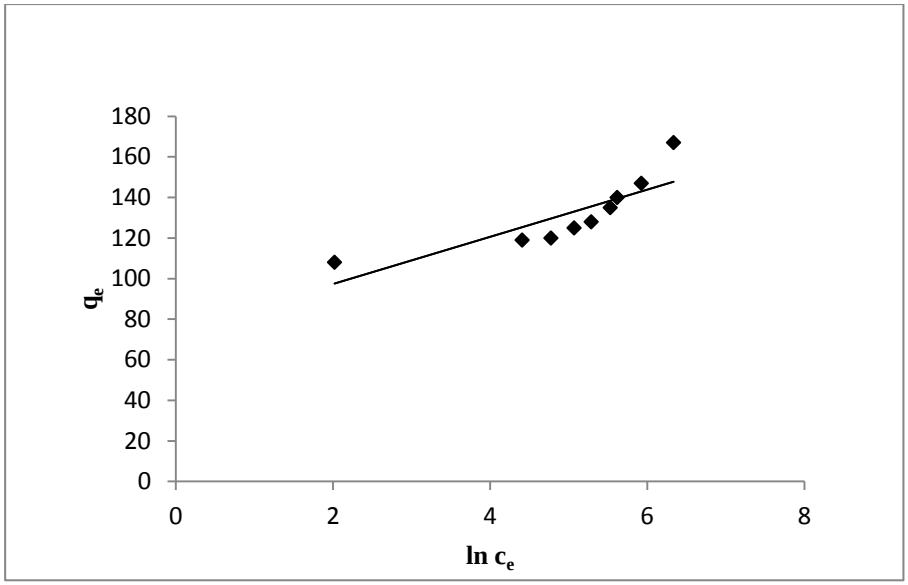

Fig. 4.22 Tempkin isotherm for removal of Cr (VI) (Solution pH 2; Dose 2.5 g/100 ml; Agitation speed 150 rpm; Temperature 35 ^{0}C)

4. 2.4 Kinetic studies

The calculated values of different kinetics parameters are presented in Table 4.8. The q_e value calculated from pseudo-first order model (Fig. 4.23) and pseudo-second order model (Fig. 4.24). The average q_e values for the pseudo-first-order model were found to be 0.83, 1.57, 1.77 and 2.73 while standard deviation values were 0.78, 1.25, 1.15 and 0.90 for the concentration ranging from 100 to 250 mg/l. R^2 values were almost more than 0.9 for all concentrations (Figure 6) which is very near to linear and comparable with experimental results. All the data follow the statistical properties and relative standard errors were found to be 46.6, 32.5, 24.5 and 12.4 for the concentration range of 100–250 ppm.

It has been found that the q_e values calculated from the pseudo-second order model are close to experimental values of q_e for all Cr (VI) concentrations. The coefficient of correlation (R^2) was also compared for all three kinetic models and it was found that the R^2value was more (near to unity) for the pseudo-second-order model. It is seen that the intra-particle diffusion model parameters increase with increasing initial Cr (VI)

concentration. The increase in the values of *I* corresponds to the increase in boundary layer thickness which gives more importance to the surface adsorption in the rate-limiting step. Since the value of *I* is not zero, this indicates the involvement of some other mechanisms in the adsorption process along with the intra-particle diffusion. The average t/q_t values for the second-order kinetic model were calculated as 1.75, 1.99, 1.84 and 1.54 for the concentration range of 100–250 ppm. Statistical analyses of data were carried out for the standard deviation and relative standard error to authenticate the findings and the values of RSE were found to be 24.1, 23.2, 23.0 and 21.5 corresponding to the concentrations of 100, 150, 200, and 250 ppm, respectively. These findings prove the results are statistically correct.

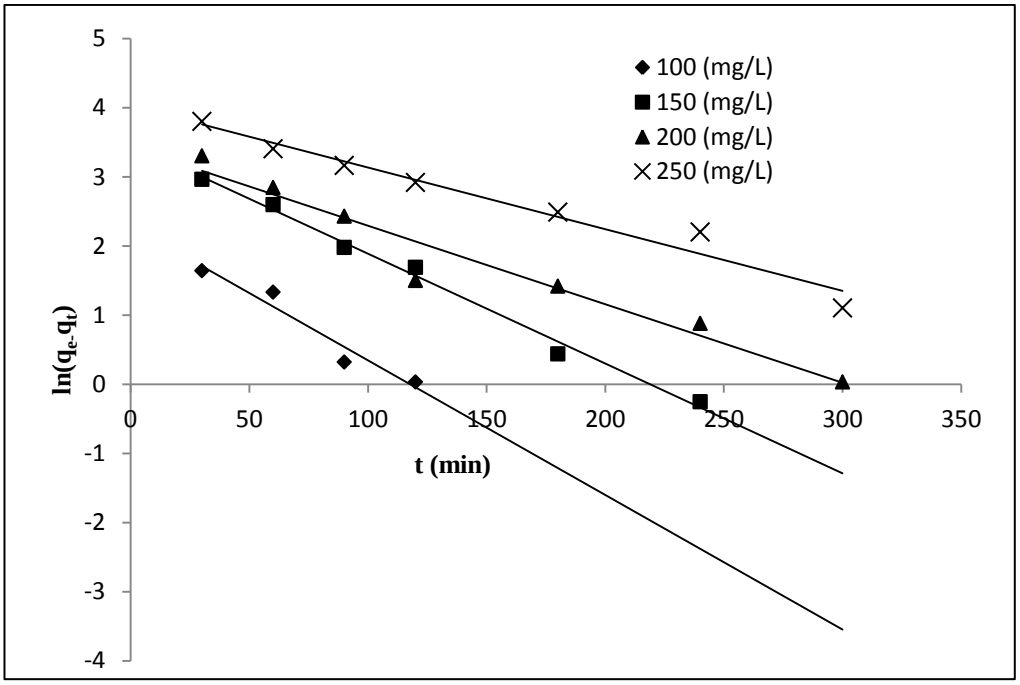

Fig. 4.23 Pseudo-first order kinetic model of Cr (VI) removal by ASAC1 (Solution pH 2; Dose 2.5 g/100 ml; Agitation speed 150 rpm; Temperature 35 ^{0}C)

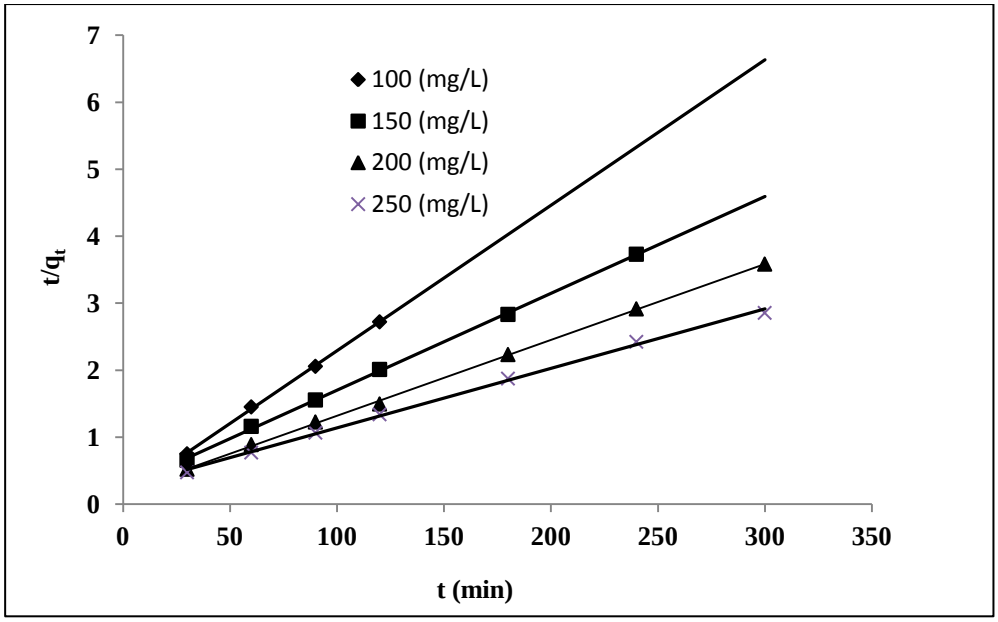

Fig. 4.24 Pseudo-second order kinetic model for Cr (VI) removal by ASAC1 (Solution pH 2, Dose 2.5 g/L; Agitation speed 150 rpm; Temperature 35 ^{0}C)

Table 4.8 Kinetics parameters of Cr (VI) adsorption on ASAC1

Kinetic parameters models	Initial concentration (mg/L)			
	100	150	200	250
q_e(exp) (mg/g)	45.12	65.103	84..73	108.072
Pseudo- first order model				
k_1	0.019	0.015	0.011	0.008
q_e(cal)	9.89	32.29	40.23	56.82
R^2	0.943	0.991	0.948	0.962
Pseudo -second order model				
k_2	0.1820	0.0546	0.0588	0.0322
q_e(cal)	47.6	71.42	90.90	125.2
R^2	0.999	0.999	0.999	0.998
Intra- particle diffusion model				
k_{id}	0.668	2.281	3.045	3.460
I	36.53	39.65	43.17	48.94
R^2	0.928	0.965	0.911	0.939

4.2.5 Regeneration study of ASAC1

Disposal of Cr (VI) loaded activated carbon is not safe because of its environmental constraints. Hence, before disposal, it must be regenerated and the activated carbon reused. The adsorption of Cr (VI) on ASAC1 is a physico-sorption process. In the present study the adsorption of Cr (VI) is highly dependent on pH value and active in the lower pH range. Hence, the regeneration of Cr (VI) is achieved by increasing the solution pH through different concentrations of NaOH (1.0, 2.0 and 2.5 M). The desorption percentages for the Cr (VI) saturated adsorbents are 25.35, 54.35 and 63.45% for ASAC1 at the three different concentrations of NaOH. The regeneration study results indicated that a higher concentration of NaOH is effective for increasing the desorption efficiency of ASAC1.

4.2.6 Thermodynamic study

The thermodynamic parameters were obtained for initial Cr (VI) concentration of 270 mg/L at pH 2. The negative value of Gibbs free energy change indicates the feasibility and spontaneity of the adsorption process on ASAC1. The enthalpy change is positive and confirms that the adsorption on ASAC1 was endothermic in nature. The positive value of ΔS shows that the adsorption process is governed by entropy rather than enthalpy. The values of ΔH^o and ΔS^o were found to be 22.9 KJ/mol and 95.3 J/mol-K. Rangabhashiyam and Selvaraju (2015) reported the negative $\Delta G°$ values showed the thermodynamically feasible and spontaneous nature of the bio-sorption process for an initial Cr (VI) concentration of 100 and 200 mg/L, but the free energy change value was found to be positive at the high Cr(VI) concentrations of 300, 400 and 500 mg/L signifying the non-spontaneous nature.

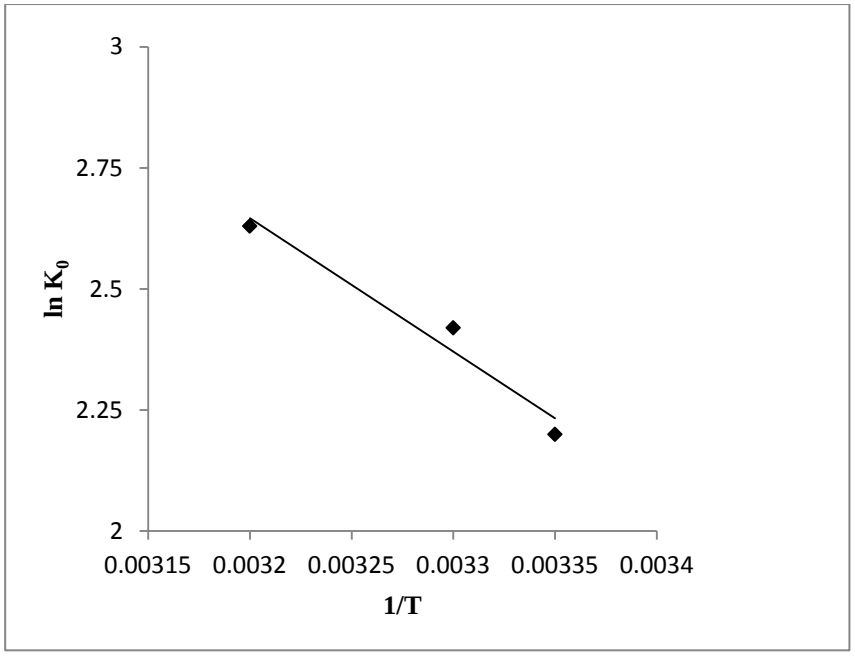

Fig. 4.25 Determination of thermodynamic properties for adsorption of Cr (VI) on almond shell activated carbon

Table 4.9 Thermodynamic parameters for the adsorption of Cr (VI) on ASAC1

Temperature(K)	ΔG° (KJ/mol)	ΔH° (KJ/mol)	ΔS° (J/molK)
298	-5.45		
303	-6.09	22.92	95.27
308	-6.73		

4.2.7 CONCLUSIONS

In the present study almond shell activated carbon was prepared by chemical activation with H_3PO_4 and carbonized at 600 °C, and used as a base material for the removal of Cr (VI). Characterization results show a very high BET surface area of 1223 m^2/g which is comparable with other activated carbon prepared from agro waste. The presence of favorable functional groups for adsorption and a highly porous structure with greater homogeneity is found which makes the prepared material a perfect

adsorbent. The characterization results were also validated with very high adsorption capacity of 202.34 mg/g under optimum operating conditions which shows the potential of the material for commercial application. The kinetic study of the adsorption process showed that the process followed pseudo-second order kinetics. The thermodynamic study revealed the endothermic nature of the process.

Section -C

4.3 Adsorption of methylene blue dye almond shell activated carbon (ASAC2)

4.3.1 Characterization of almond shell activated carbon (ASAC2)

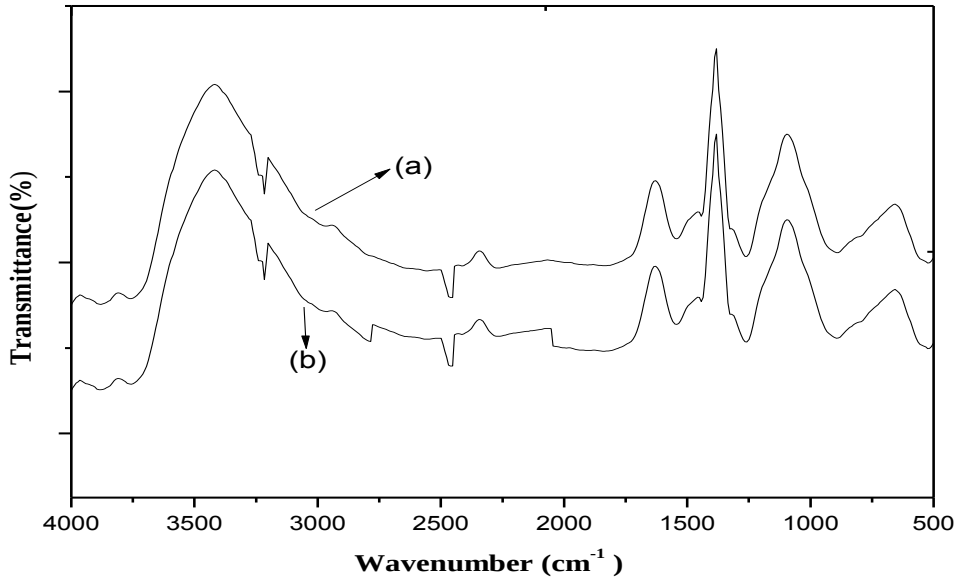

Fig. 4.26 FT-IR spectra of activated carbon before (a) and after adsorption (b) of MB

The FTIR spectra of adsorbent material from almond shell at initial stage and after MB uptake were recorded in the spectral range of 500- 4000 cm^{-1} and are presented in Fig. 4.26. The peaks observed at 2796 and 3900 cm^{-1} are related to O-H functional groups like alcohols and carboxylic acids (Li et al., 2016; Das et al., 2015, Uner, 2019). The spectral peaks around 850–500 cm^{-1} confirms to C-H and CH_2=CH_2 stretching groups (Gupta et al., 2011; Mamania et al., 2019). The band seen at 1748 and 1650 cm^{-1} could be represent to the C-O and COO- stretching groups respectively vibrations in aromatic structures (Xu et al., 2013; Mahamad et al., 2015, Zhang et al., 2019). FTIR

spectra after adsorption on ASAC2 is indicated the shifted peak locations and low transmittance intensity at some bands due to MB attachment in pores of activated carbon.

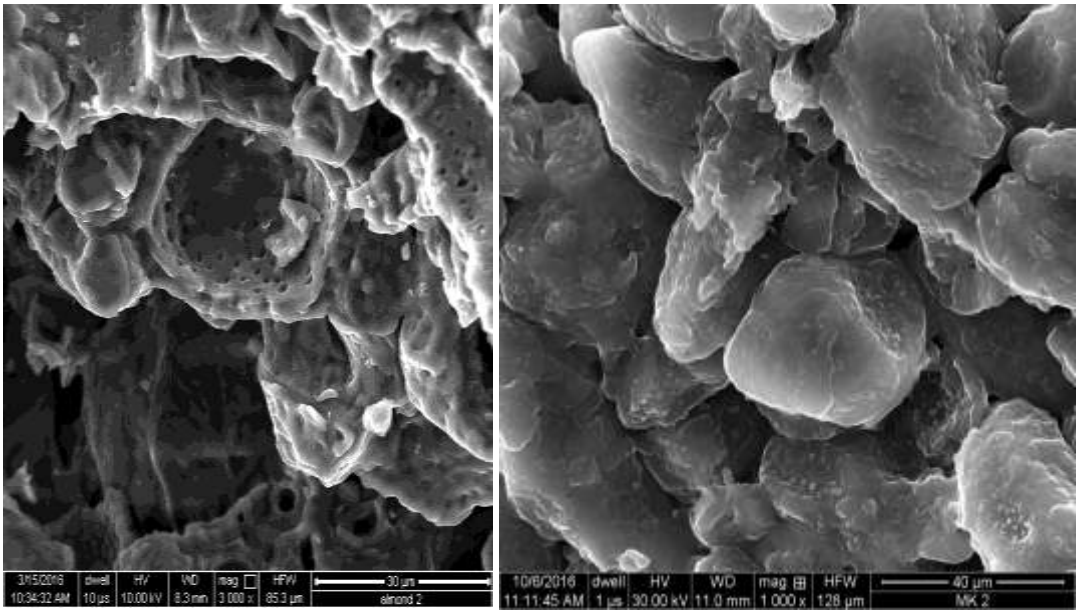

Fig. 4.27 SEM image of activated carbon before (a) and after adsorption (b) of MB

The observed SEM images of ASAC2 are presented in Fig. 4.27. The role of H_3PO_4 to generate the porous structure of ASAC2 is observed on the surface. The appearance of porosity is due to dehydration which breaks the different bond like C-C and C-O-C of almond shell during activation. The SEM image after MB adsorption shows that the pores are filled by MB adsorption on the surface and in the pores of activated carbon.

From elemental analysis of almond shell (Table 4.10) it is seen that the higher percentage of carbon (76.40%) in activated carbon. The same type of results were investigated by other activated carbon like hazelnut-husk (80.4 %) (Karacetin et al., 2014) and sugar beet bagasse (70–80 %) (Onal et al., 2007).

The surface area of ASAC2 is found to be 1250 m^2/g and pore volume is found to be 0.3885cm^3/g. This results is compared with other activated carbons such as tapioca flour (Pari et al., 2014) and orange peels (Fernandez et al., 2015) having 986 and 618 m^2/g BET surface areas and total pore volumes 0.57 and 0.39 cm^3/g, respectively. The physical characterization like average pore size and point of zero charge of ASAC2 were found to be 2.47 nm and 5.50 (Table 4.10) respectively which can take role in adsorption capacity.

Table: 4.10 Physical properties of almond shell activated (ASAC2) carbon.

Parameters	**Value**
BET Surface area (m^2 g^{-1})	1250
Pore volume (cm^3 g^{-1})	0.3885
Average pore size (nm)	2.47
pH at the point of zero surface charge (pHpzc)	5.5
Elemental analysis (%)	
C	76.40
H	2.40
N	1.38
S	0
O	19.82

4.3.2Effect of initial pH of MB

The starting pH of any dye effluent is an adequate parameter to investigate uptake capacity of any absorbent and it is also important to investigate the removal effect of activated carbon (Hameed et al., 2007). The role of pH for MB uptake (Fig. 4.28) onto ASAC2 was performed at various solution pH ranges (2-11), 0.25/100 mL of ASAC2 dosage, initial concentration of dye as 100 mg/L and 30 ºC for 6 h. The adsorption

efficiency was less in acidic range (pH 2 to 6), but it was observed maximum under basic conditions above pH 7. The reason for this behaviour is due to basic nature of MB dye having positive ions in solution (Aljeboree et al., 2015; Tan et al., 2007). The adsorbent surface which is positively charged in acidic range will not attract cationic MB molecules. After increasing the pH from 2 to 7 the surface of ASAC2 will get negatively charged ions which accumulated the positive MB ions (Khan et al., 2015).

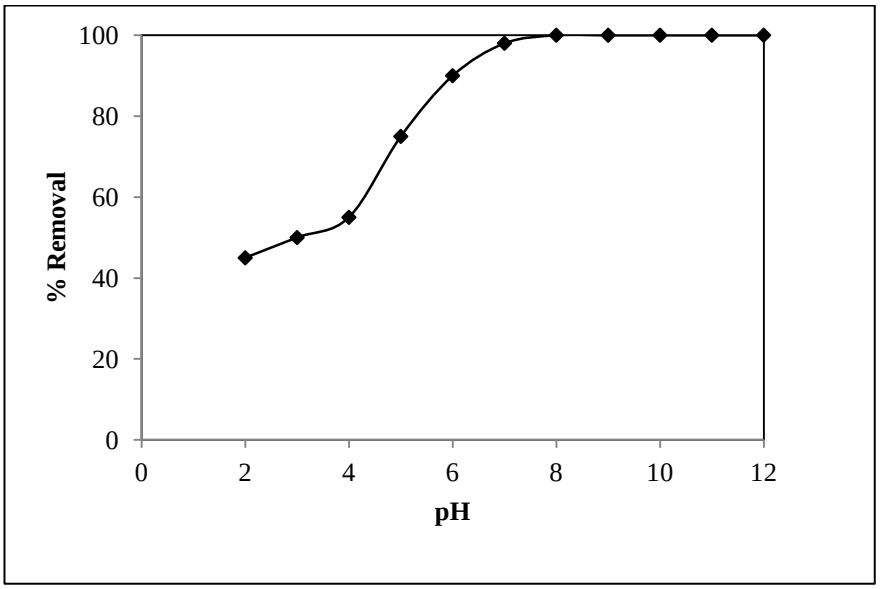

Fig. 4.28 Effect of Initial pH of solution on MB removal (Initial conc.: 100 mg/l; Contact time 360 min; adosrbent dose 0.25 g/100 ml; Agitation speed: 180 rpm; Temperature: 30˚C)

4.3.3 Adsorbent dose and time variation

To investigate the effect of adsorbent dose and running time on uptake, the operating parameters was taken as dose in range of (0.2-0.8 g/100 mL), solution pH 7 and initial MB concentration of 100 mg/L. During first 150 min of contact time the adsorption uptake incenses exponentially but after 240 minuses the change in uptake becomes constant. This phenomenon is due to various numbers of free adsorptive locations on the ASAC2 during initial, but after MB adsorption the availability of vacant sites decreases which results low uptake on ASAC2 (Nasrullah et al., 2018;

Pathania et al., 2017). MB removal efficiency was changed according to variation ASAC dose (Naeem et al., 2017). Form fig. 4.29 it is clear that the MB uptake is 10mg/g at ASAC2 dose of 0.8g/100 mL and it becomes 50 mg/g at dose of 0.2g/100mL

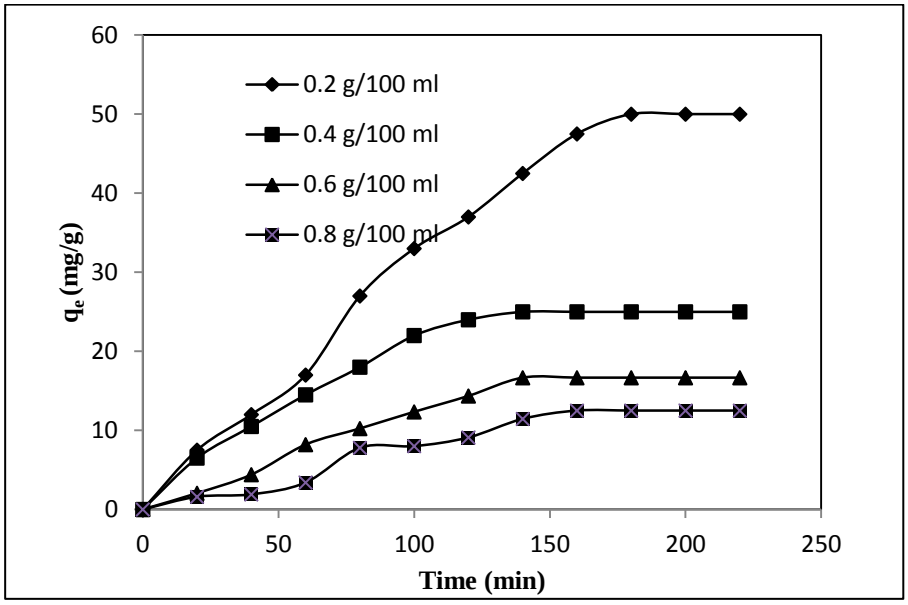

Fig. 4.29 Effect of adsorbent dose Methylene blue uptake (Initial conc.: 100 mg/L; Solution pH 7; Agitation speed: 180 rpm; Temperature: 30˚C)

At higher ASAC2 dose the MB uptake is low because high percentage of ASAC2 in compression to MB dye and ASAC2 remains unsaturated (Bulut and Aydin , 2006; Liu et al., 2016). Therefore foe next experiments the ASAC2 dose is takes as 0.2g/100 mL.

4.3.4Effect of initial MB concentration

The concentration of MB dye effects the adsorption percentage removal. For this percentage removal and uptake of MB versus initial MB concentration are presented in the Fig. 4.30 for the concentration range of 50 mg/L -800 mg/L. It is carried out from the figure that the removal of MB dye is 100% up to 100 mg/L, MB concentration and it is decreased reaching 75% at 800 mg/L MB concentration. The q_e value of by the ASAC2 increases by increasing MB concentration and it is reached at good adsorption

uptake value of 270 mg/g for 800 mg/L MB concentration. The reason for this is the mass transfer resistance which is affected at different MB concentration by interaction with solid phase ASAC2. At higher concentration of MB increases the interaction of MB molecules on the surface of ASAC2 which gives high value of dye uptake (Mahmoud et al., 2012; Islam et al., 2015). The same type of result has been got by waste rice activated carbon (Sangon et al., 2018) and nanoporous carbon (Han et al., 2018).

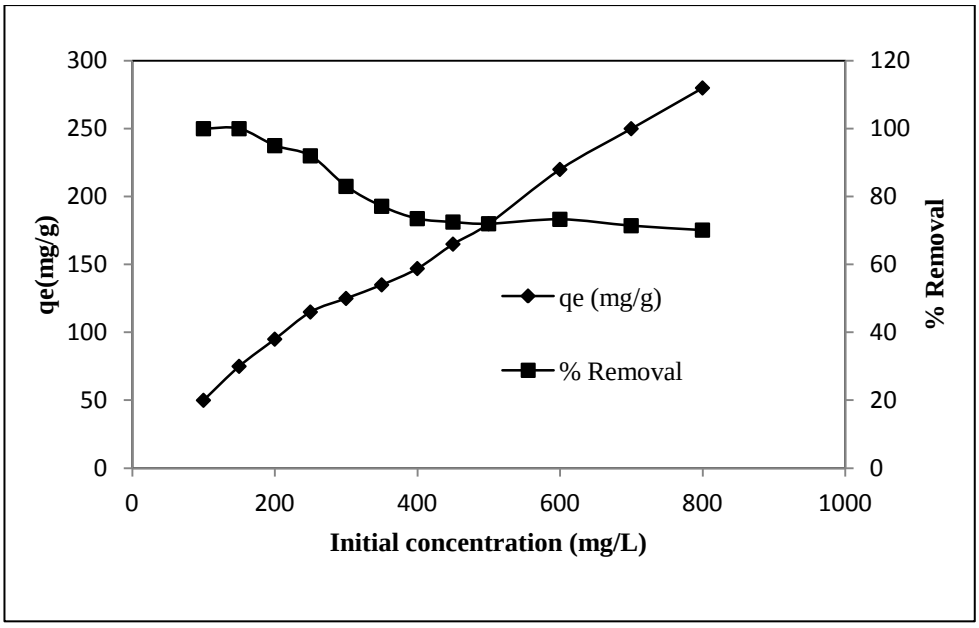

Fig. 4.30 Effect of initial MB concentration (Solution pH: 2; Agitation speed: 180 rpm; Dose: 0.2g/100ml; Temperature 30˚C; Time: 240 min)

4.3.5Adsorption isotherm

For the determination of adsorption mechanism, the adsorption isotherm is preferred analysis. This analysis indicates how the liquid phase containing adsorbate molecules are spread on the surface of adsorbent and liquid phase. The values of adsorption isotherm are useful to carry out the suitable isotherm model that may help in design findings. To investigate the best adsorption isotherm model four models like as the

Langmuir, Freundlich, Temkin and Dubinin–Radushkevich were tested in present experiments. The suitable isotherm models were compared by relating the correlation coefficients, R^2 in this study.

The adsorption isotherms for all four models are inserted in Fig. 4.31 to 4.34 and the calculated results of all the four isotherms are presented in Table 4.11. The best fit for four isotherms were selected on the basis of the highest correlation coefficient (R^2) value (closer to 1) for the experimental observed values. Form the graph the value of R^2 for Langmuir model was estimated to 0.998 which was more in compression to other isotherm models. This data confirmed the monolayer adsorption of methylene blue by lagmuir model on ASAC2. The maximum uptake (q_m) determined by Langmuir model is 334.40 mg/g at temperatures 30 ºC which is related to experimental value and comparable with other activated carbon such as corncob (Ma et al., 2015). The calculated R_L values are less than one for concentration ranging 50 mg/L to 1000 mg/L which confirms that the removal of methylene blue is favourable on ASAC2. For freundlich isotherm the constant value, 1/n is less than unity which refers the adsorption process is possible but the vale correlation coefficient (R^2 =0.974) is less than as compared to lagmuir isotherm. Table 4.11 presents the comparison of maximum uptake of MB by different activated carbons.

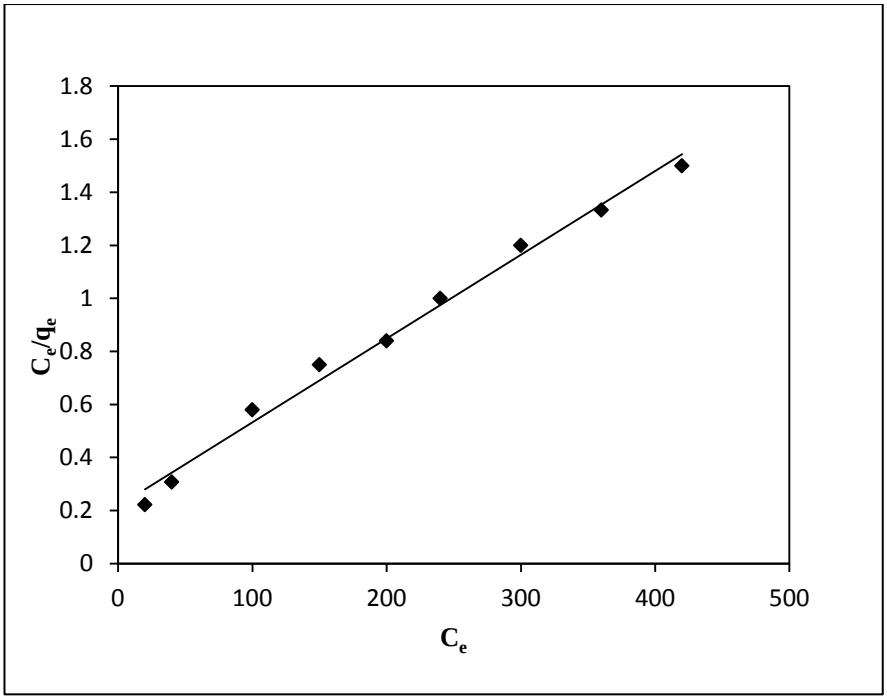

Fig. 4.31 Adsorption isotherms for MB adsorption- Langmuir- (Solution pH: 2; Agitation speed: 180 rpm; Dose: 0.2g/100mL; Temperature 30˚C; Time: 240 min)

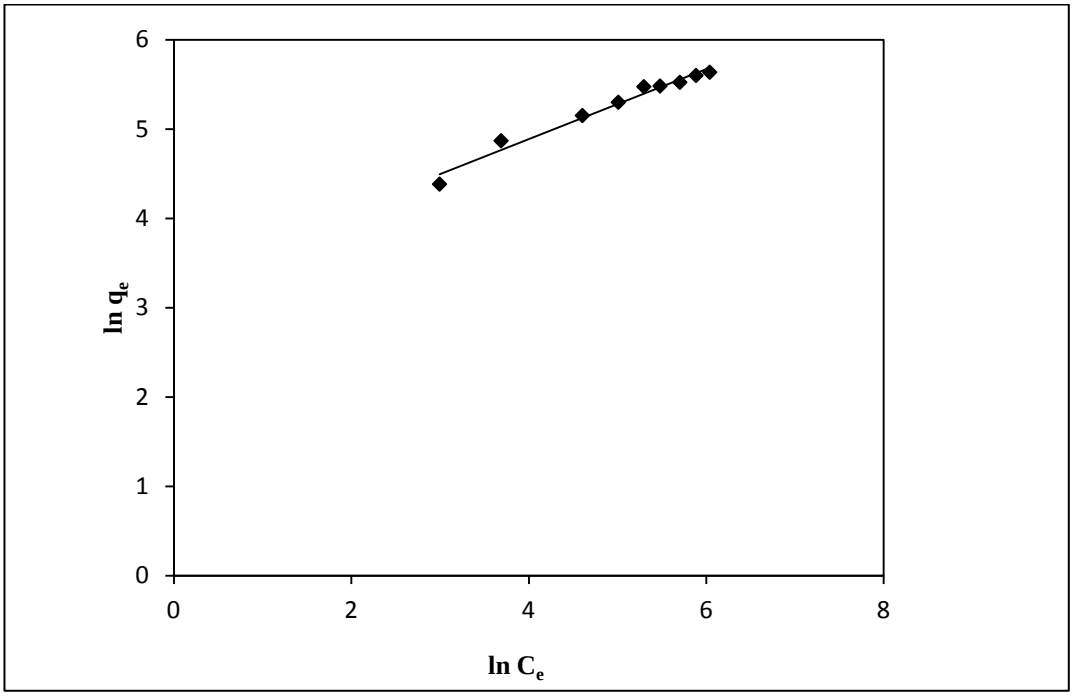

Fig. 4.32 Adsorption isotherms for MB adsorption- Freundlich isotherm (Solution pH: 2; Agitation speed: 180 rpm; Dose: 0.2g/100 mL; Temperature 30˚C; Time: 240 min)

Tempkin isotherm constant A_T and b_T are obtained by plotting the curve between q_e verses ln C_e and presented in table 4.11. The R^2 (0.987) value for Termkin isotherm is less in comparison to Lagmuir isotherm. The maximum absorption capacity q_m and R^2 values obtained from D-R model are 269.88 mg g^{-1} and 0.911. The obtained q_m and R^2 values for D-R model are less in comparison to Langmuir isotherm model (334.40 mg g^{-1} and 0.998). The energy of adsorption (E) is observed as 7.071 kJ mol^{-1} (E< 8.0 kJ mol^{-1}). This value of E correlates that the adsorption mechanism is followed by physisorption.

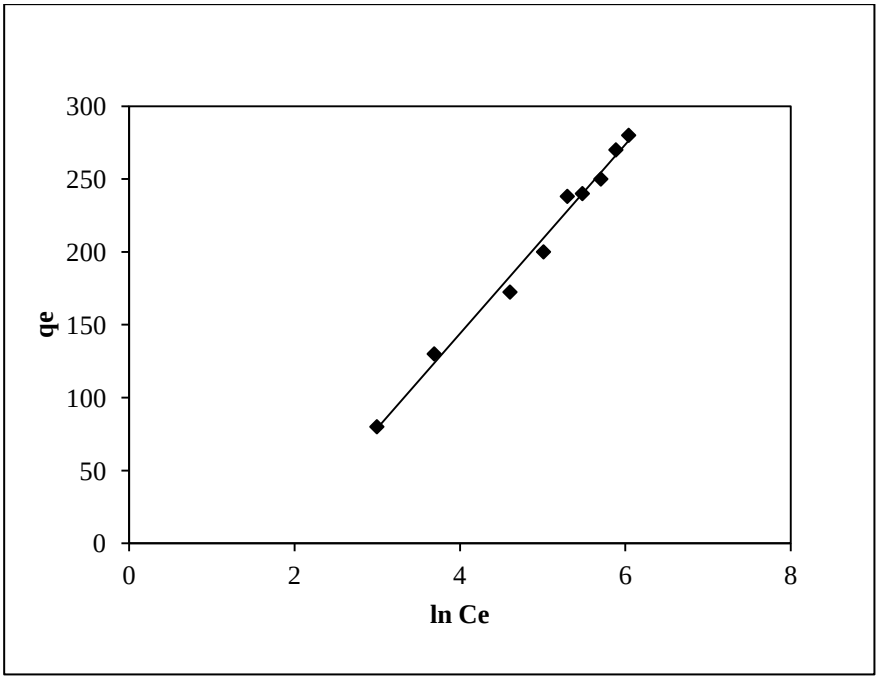

Fig. 4.33 Adsorption isotherms for MB adsorption – Tempkin isotherm (Solution pH: 2; Agitation speed: 180 rpm; Dose: 0.2g/100mL; Temperature 30˚C; Time: 240 min)

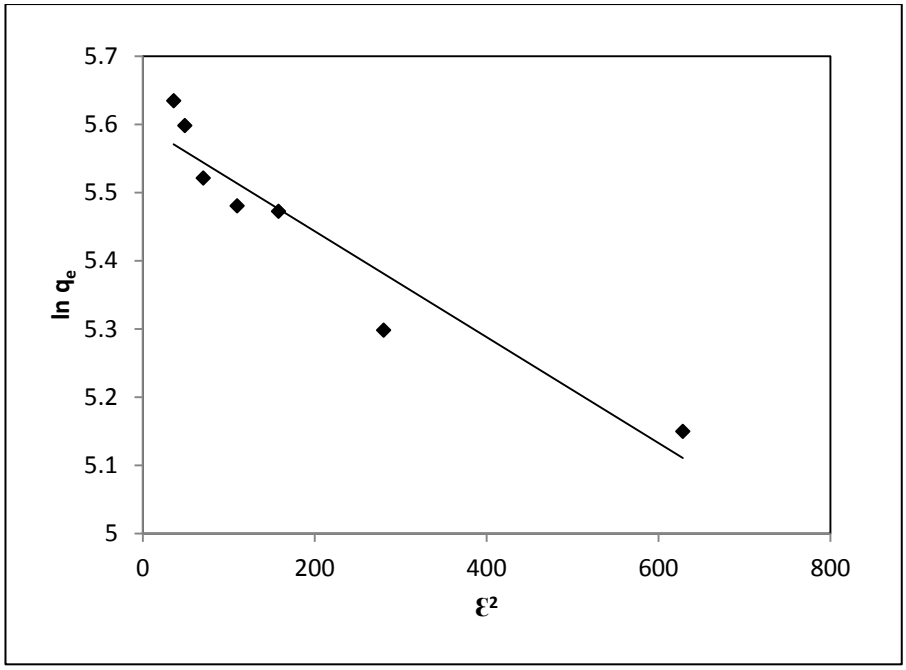

Fig. 4.34 Adsorption isotherms for MB adsorption- Dubinin and Radushkevich isotherm (Solution pH: 2; Agitation speed: 180 rpm; Dose: 0.2g/100 mL; Temperature 30˚C; Time: 240 min.)

Table 4.11 Isotherm parameters for MB adsorption on ASAC2

Adsorption isotherm	**Parameters**	**Values at 30 ^{0}C**
Langmuir isotherm	q_m	334.40
	b	0.0134
	R^2	0.998
	R_L	0.790
Freundlich isotherm	K_f	27.549
	n	2.550
	R^2	0.974
Tempkin	A_T	0.1686
	b_T	38.79
	R^2	0.987
Dubinin-Radushkevich	q_m	269.88
	K	0.0001
	E	7.071
	R^2	0.911

4.3.6 Kinetic study

For the determination of the kinetic parameters of removal, the value of equilibrium data was fitted to different kinetics model. For investigating the MB adsorption kinetics, the experiments were performed at various initial concentrations of MB at pH 7, temperature of 30 ºC, adsorbent dose of 2.5 g/L and adsorption time of 240 min.

The observed data of different kinetic parameters are tabulated in Table 4.12. The uptake q_e and rate constant are explained for the three kinetic modes such as pseudo-first order, pseudo- second order and intra - particle diffusion mode. Fig. 4.36 is plotted for different initial concentrations of 100, 200 and 300 mg/l and different time range. The correlation coefficient for pseudo second order and intra particle diffusion model is calculated by linear equation. It was the coefficient of correlation as 0.961, 0.9707 and 0.985 for intra particle diffusion model. The data of correlation coefficients obtained from this linear equation of the pseudo-second order model are closer to unity (R^2>0.99) for different initial MB concentration (100 mg/L-300 mg/L) in compression the pseudo-first order model (R^2>0.91) and intra-particle diffusion model, which reveals that the pseudo-second order model is suitable to design kinetics and rate of adsorption. Also the calculated value of uptake ($q_{e,\ cal}$ =138.60 mg/g) is comparable to experimental uptake ($q_{e,\ exp}$ = 130.50 mg/g) for this model which confirms that second order kinetic model is responsible for the MB uptake on ASAC2.

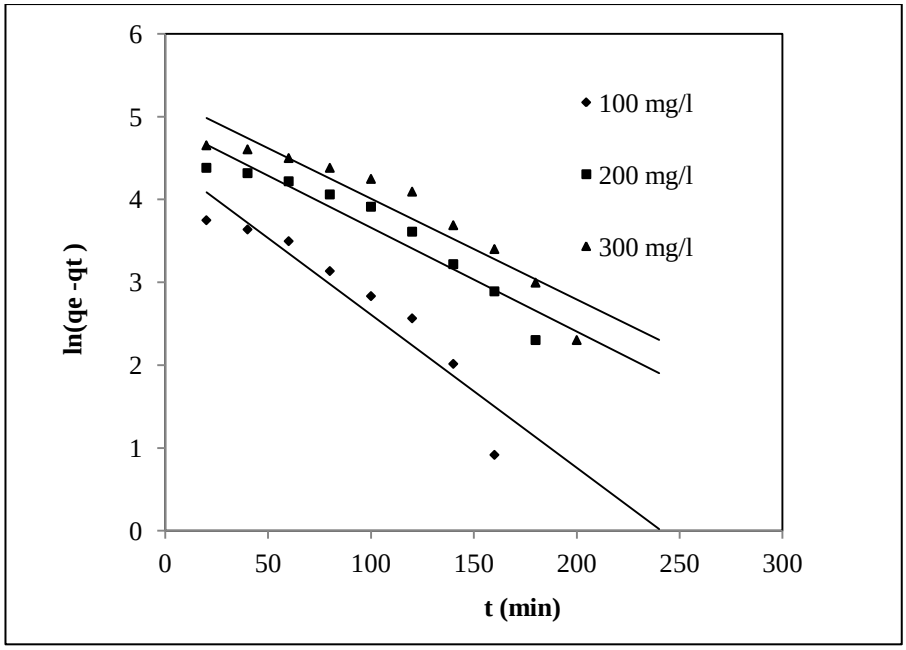

Fig. 4.35 Adsorption kinetics models for MB adsorption - Pseudo first- order(Solution pH: 2; Agitation speed: 180 rpm; Dose: 0.2g/100mL; Temperature 30˚C; Time: 240min.; Initial con. of MB: 100, 200 and 300 mg/L)

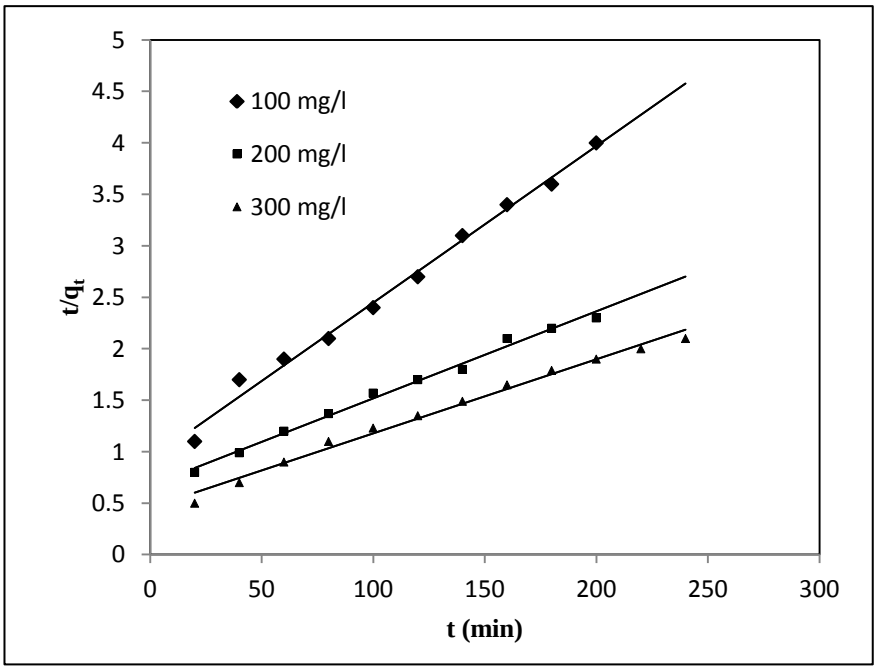

Fig. 4.36 Adsorption kinetics model for MB adsorption - Pseudo second- order (Solution pH: 2; Agitation speed: 150 rpm; Dose: 0.2g/100mL; Temperature: 30˚C; Time: 240min.; Initial con. of MB: 100, 200 and 300 mg/L)

Table 4.12 Kinetics parameters for adsorption of MB

Kinetic parameters models	Initial concentration (mg/L)		
	100	200	300
q_e(exp) (mg/g)	50.0	90.70	130.50
Pseudo- first order model			
k_1	0.018	0.012	0.013
q_e(cal)	86.142	135.77	185.86
R^2	0.890	0.915	0.891
Pseudo -second order model			
$k_2 \times 10^{-4}$	2.43	9.5	1.13
q_e(cal)	66.50	110.5	138.60
R^2	0.991	0.992	0.998
Intra- particle diffusion model			
k_{id}	3.437	5.710	6.284
I	4.428	5.402	16.74
R^2	0.961	0.9707	0.985

4.3.7 Thermodynamic study

The thermodynamic properties were calculated from the graph (Fig.4.37) between ln K_0 and 1/T. The calculated thermodynamic propertied such as (ΔG°, ΔH° and ΔS°) were presented in Table 4.13. The negative value of Gibbs free energy is increased from -19.69 KJ/mol to -21.53 KJ/mol with increasing temperature from 298K to 308 K, which indicated the fissile and spontaneous adsorption process of MB on almond shell activated carbon. The positive value of entropy change (ΔH° = 35.11 KJ/mol) confirmed the endothermic adsorption process of MB, which favors the adsorption of MB at higher temperature. The entropy changed (ΔS°=183.73 J/mol K) is positive which refers the increased randomness at solid/liquid interface.

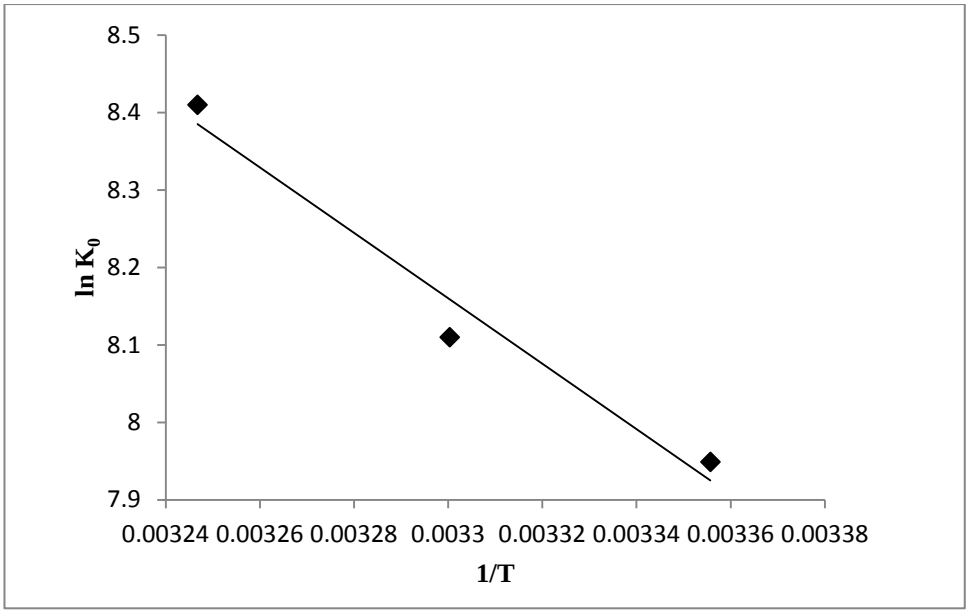

Fig. 4.37 Determination of thermodynamic parameters for adsorption of MB on almond shell activated carbon

Table 4.13 Thermodynamic parameters of MB adsorption on almond shell activated carbon

Temperature(K)	ΔG° (KJ/mol)	ΔH° (KJ/mol)	ΔS° (J/molK)
298	-19.69		
303	-20.42	35.11	183.73
308	-21.53		

4.3.8 Conclusion

Almond shell wastes were used as feed stock for the preparation of activated carbon which was highly porous in nature and having high surface area by chemical activation with H_3PO_4 and carbonized at 700 °C. The surface area of ASAC2 by BET method was calculated as 1250 m^2/g with different functional group which was responsible for MB uptake. The prepared ASAC2 was utilized as an economical and easily available adsorbent for removal of MB dye having high adsorption extent of 333.34 mg/g at 30 ºC which is more than in compression to many other activated carbon. The calculated

equilibrium data of MB adsorption onto ASAC2 were best explained by Langmuir isotherm model and the MB removal kinetics were evaluated and designed by pseudo-second order kinetic model. The positive value of entropy change (ΔH° = 35.11 KJ/mol) confirmed the endothermic adsorption process of MB.